Journal Pre-proofs

Unravelling the interactions between small molecules and liposomal bilayers via molecular dynamics and thermodynamic modelling

Christopher M. Miles, Shane Cullen, Hussein Kenaan, Wenjie Gu, Gavin P. Andrews, Gabriele C. Sosso, Yiwei Tian

PII: S0378-5173(24)00601-X
DOI: https://doi.org/10.1016/j.ijpharm.2024.124367
Reference: IJP 124367

To appear in: *International Journal of Pharmaceutics*

Received Date: 10 April 2024
Revised Date: 6 June 2024
Accepted Date: 17 June 2024

Please cite this article as: C.M. Miles, S. Cullen, H. Kenaan, W. Gu, G.P. Andrews, G.C. Sosso, Y. Tian, Unravelling the interactions between small molecules and liposomal bilayers via molecular dynamics and thermodynamic modelling, *International Journal of Pharmaceutics* (2024), doi: https://doi.org/10.1016/j.ijpharm.2024.124367

Unravelling the Interactions Between Small Molecules and Liposomal Bilayers via Molecular Dynamics and Thermodynamic Modelling

Christopher M. Miles,[1] Shane Cullen,[2] Hussein Kenaan,[2] Wenjie Gu,[2] Gavin P. Andrews,[2] Gabriele C. Sosso,[1*] Yiwei Tian,[2*]

[1] Department of Chemistry, University of Warwick, Coventry, CV4 7AL, United Kingdom

[2] School of Pharmacy, Queen's University Belfast, 97 Lisburn Road, Belfast BT9 7BL, United Kingdom

Corresponding authors: y.tian@qub.ac.uk; g.sosso@warwick.ac.uk;

Abstract

Lipid-based drug delivery systems hold immense promise in addressing critical medical needs, from cancer and neurodegenerative diseases to infectious diseases. By encapsulating active pharmaceutical ingredients – ranging from small molecule drugs to proteins and nucleic acids – these nanocarriers enhance treatment efficacy and safety. However, their commercial success faces hurdles, such as the lack of a systematic design approach and the issues related to scalability and reproducibility.

This work aims to provide insights into the drug-phospholipid interaction by combining molecular dynamic simulations and thermodynamic modelling techniques. In particular, we have made a connection between the structural properties of the drug-phospholipid system and the physicochemical performance of the drug-loaded liposomal nanoformulations. We have considered two prototypical drugs, felodipine (FEL) and naproxen (NPX), and one model hydrogenated soy phosphatidylcholine (HSPC) bilayer membrane. Molecular dynamic simulations revealed which regions within the phospholipid bilayers are most and least favoured by the drug molecules. NPX tends to reside at the water-phospholipid interface and is characterized by a lower free energy barrier for bilayer membrane permeation. Meanwhile, FEL prefers to sit within the hydrophobic tails of the phospholipids and is characterized by a higher free energy barrier for membrane permeation. Flory-Huggins thermodynamic modelling, small angle X-ray scattering, dynamic light scattering, TEM, and drug release studies of these liposomal nanoformulations confirmed this drug-phospholipid structural difference. The naproxen-phospholipid system has a lower free energy barrier for permeation, higher drug miscibility with the bilayer, larger liposomal nanoparticle size, and faster drug release in the aqueous medium than felodipine. We suggest that this combination of molecular dynamics and thermodynamics approach may offer a new tool for designing and developing lipid-based nanocarriers for unmet medical applications.

1. Introduction

Phospholipids, ubiquitously in nature, are amphiphilic molecules consisting of a polar, hydrophilic group and two apolar, hydrophobic fatty acid side chains. In the presence of aqueous solutions, phospholipids spontaneously form micelles or bilayer membranes to minimize the interactions between hydrophobic groups, leading to the self-assembly of lipid-based nanoparticles (LNP) or liposomes (Beltrán-Gracia et al., 2019; Peer et al., 2007; Xing et al., 2016). These nanocarriers with a size range between 20 to 200 nm can offer unique chemical and biological features for diagnosing, monitoring, preventing, and treating unmet clinical conditions (Farokhzad and Langer, 2009). As one of the most promising strategies for nanoparticle drug delivery, liposomes have been continuously researched for encapsulating a wide range of active pharmaceutical ingredients (APIs), including small molecules, proteins, peptides, and peptide nucleic acids, to tumours or sites of inflammation (Kluzek et al., 2022; Shi et al., 2017). Other modifications for LNPs were also developed to enable different delivery mechanisms, such as passive targeted delivery (Pereira et al., 2022), PEGylated long-circulating stealth system, and chemical responsive drug release (Barenholz, 2012). Specific efforts have focused on drugs that are difficult to deliver due to low water solubility and high toxicity (Bakshi et al., 2018; Giardiello et al., 2016). Therapeutics and diagnostics in cancer (Barenholz, 2012; Janssen products, 2013), neurodegenerative diseases (Kabanov, A V; Gendelman, 2007), diabetes (Tromans et al., 2018; Veiseh et al., 2016), infectious diseases (Bern et al., 2006; Meyerhoff, 1999), and inflammation (Schiener et al., 2014) have already benefited from nanotechnology. Recent successful clinical delivery of the COVID-19 vaccine and short interfering RNA (siRNA) are the two landmarks for LNP drug delivery systems (Akinc et al., 2019; Hou et al., 2021; Kisby et al., 2021). Encapsulation of APIs in an LNP or liposome can dramatically alter the distribution by controlling the release to normal tissue while facilitating the accumulation at the desired targets. In the systemic circulation and distribution to tissue/organ, the release kinetics of the encapsulated payloads are often critical to the safety and efficacy of the treatment (Tang et al., 2019). An adequately designed liposomal bilayer can offer suitable API retention and stability for therapeutic purposes. While significant progress has been made to foster such a drug delivery system, the lack of a systematic approach to the entire design space of liposomes has partly hindered the wide clinical applications. Heavily researched lipid-based nanoformulation designs inherited from previously marketed products or drug delivery experts often rely on only a few design principles. Subsequently, many mimicking nanoformulations were utilized for new APIs, often in vain at the clinical trial stage (Park, 2016, 2013). The structural-response relationships in the initial nanocarrier design space, the interactions with the payload, and the critical quality attributes of the finished nanoformations are poorly understood. Limited research, often based

on simple and/or empirical experiment approaches, has resulted in negligible outcomes in improving the final clinical efficacy of nanomedicines. For example, the variables of the nanocarrier, e.g., phospholipid type, composition, size, and ionic strength, and the complexity and heterogeneity of the microenvironment at the target still present significant challenges and opportunities in this field (Bonnans et al., 2014; Shi et al., 2017). To provide a detailed understanding of both structural and physicochemical drug-phospholipid interactions, several biophysical techniques have been developed through membrane models at the air-liquid and solid-liquid interfaces (Clifton et al., 2020). Many advanced characterization techniques can assist such understanding of the drug, lipid-based nanocarriers, and their interfaces, such as nuclear magnetic resonance, small angle x-ray/neutron scattering, and cryo-EM or liquid-EM (Jabbari et al., 2023; Yao et al., 2020). A recent development in x-ray/neutron scattering and surface-sensitive imaging techniques can provide visualized understanding with incredibly high resolutions (Paracini et al., 2023).

From a computational standpoint, molecular dynamics (MD) simulations can provide a mechanistic understanding of the interactions between the drug and the lipid-based nanocarriers. In recent years, coarse-grained (CG) MD has often been used to build and characterize model phospholipid systems (Bunker et al., 2016). In contrast to fully atomistic MD, CG-MD allows access to longer/larger time-/length-scales, as it clusters groups of atoms into so-called "beads", significantly reducing the computational costs of these simulations. Unsurprisingly, however, this approach comes at the expense of sacrificing accuracy to some extent. Representative examples of CG-MD would include the model of Parchekani *et al.* to investigate the structural and dynamical properties of liposomes coated with polyethene glycol (PEG), their sensitivity to pH, and the impact of external stimulations (e.g. ultrasound or heat) on the release of drug molecules in liposomes (Parchekani et al., 2022). MD studies simulating the actual drug release mechanism are also beginning to emerge in recent literature. For instance, Marcos *et al.* studied the incorporation of N-(2-hydroxyphenyl)-2-propylpentanamide in dimyristoyl-phosphatidylcholine (DMPC) liposomes in the presence or absence of cholesterol (CHOL) (Marcos et al., 2022); Siani *et al.* investigated the penetration of doxorubicin in liposome membranes modelled as phosphatidylcholine (PC)/sphingomyelin (SM)/CHOL lipid bilayers (Siani et al., 2022) and Jämbeck *et al.* simulated the release of hypericin from a liposome model (Jämbeck et al., 2014). A notable example of Monte Carlo simulations was also used to understand the drug release through liposomal pores (Dan, 2015). It is clear that the combination of MD simulations with advanced characterization techniques can improve our understanding of the drug-phospholipid interface and represents a new systemic tool for designing and developing new lipid-based drug delivery vesicles.

This study combined fully atomistic MD simulations with thermodynamic modelling and experimental characterization to provide a comprehensive picture of the drug-phospholipid interactions, including the drug encapsulation and release from the liposomal nanocarriers. Specifically, the molecular-level details of the drug-phospholipid interactions are investigated via enhanced sampling simulations based on MD, whilst the phase behaviours of the drug-phospholipid binary mixtures are explored via Flory-Huggins based thermodynamic modelling. Furthermore, the importance of drug encapsulation and phase behaviours obtained from the modelling were highlighted in relation to the physicochemical performance of the manufactured drug-encapsulating liposomal nanocarriers. Thus, this work lays the foundations for a rational approach to designing, developing, and realizing lipid-based nanocarriers, which would directly impact the nanoformulation of small molecule drugs within the early discovery phase.

2. Materials and Methods

2.1 Material

Hydrogenated soybean phosphatidylcholine (HSPC), 1,2-distearoyl-sn-glycero-3-phosphocholine (DSPC), 1,2-dipalmitoyl-sn-glycero-3-phosphocholine (DPPC) and 1,2-dimyristoyl-sn-glycero-3-phosphocholine (DMPC) were purchased from Lipoid Ltd. (Germany). Cholesterol, α-tocopherol, xylitol and disodium ethylenediaminetetraacetate (EDTA) were purchased from Sigma Aldrich (UK). Methanol, dimethyl sulfoxide (DMSO), trifluoroacetic acid (TFA), chloroform, acetonitrile, and tetrahydrofuran (THF) at analytical grade were purchased from Sigma Aldrich (Gillingham, UK) and used as received. Naproxen (purity > 98%) was purchased from Kemprotec (Cumbria, UK), and felodipine was acquired from Molekula (purity > 99%, Darlington, UK)

2.2 Methods

2.2.1 Molecular dynamics simulations

Molecular dynamics simulations were performed via the MD package GROMACS (Abraham et al., 2015; Pronk et al., 2013). The force field used to model the lipids and drug molecules was CHARMM36 (Soteras Gutiérrez et al., 2016; Vanommeslaeghe et al., 2010), whilst the TIP4P/Ice model was used to represent the water molecules (Abascal et al., 2005a). It is worth mentioning that CHARMM36 was parameterized initially to be utilized with the TIP3P water model; however, the combination of CHARMM36 and TIP4P/Ice has been extensively validated, particularly in the context of reproducing the properties of liquid water at the interface with complex biological systems in recent studies (Abascal et al., 2005b; MacKerell et al., 1998; Midya and Bandyopadhyay, 2014; Nutt and Smith, 2007). CHARMM-GUI and CGenFF were used to craft topologies and initial configurations of the lipid belayers and the

drug molecules, respectively (Brooks et al., 2009; Jo et al., 2009, 2008; Lee et al., 2016). The SETTLE and LINCS algorithms were used to constrain the geometry of the water molecules and the bond lengths of covalent bonds involving the H atom (high-frequency vibrational motion) (Hess et al., 1997; Miyamoto and Kollman, 1992). An initial energy minimization was carried out, bringing the maximum force acting on a given atom below 100 kJ mol^{-1} nm^{-1}. Three-dimensional periodic boundary conditions (PBCs) were used. Subsequently, an initial equilibration run (20 ns) was conducted at 328.15 K, sampling the canonical (NVT) ensemble. A leap-frog integrator with a timestep of 2 fs was used to integrate the equations of motion. The Bussi-Donadio-Parrinello thermostat and the Berendsen barostat were used, enforcing a surface tension coupling where relevant (Berendsen et al., 1984; Bussi et al., 2007). The cutoff for the van der Waals and electrostatic interactions was set to 12 Å. The van der Waals interactions were switched to zero between 10 and 12 Å.

Following this initial equilibration MD run, the simulation box was elongated in the z-direction up to 270 Å , creating water-vacuum interfaces to avoid artefacts caused by the slab geometry of the system – following the well-known approach of Yeh and Berkowitz (Yeh and Berkowitz, 1999). An equilibration run of 20 ns, sampling the (NVT) ensemble at 328.15 K, was then carried out. Following the NVT run, a longer NPT run of 200 ns was carried out to equilibrate the system. In these simulations, the X and Y (in-plane) box dimensions were coupled and allowed to change to accommodate the natural pressure fluctuations of the system, whilst the Z box dimension was fixed (semi-isotopic pressure coupling). As lipid bilayers can expand and contract significantly under pressure, we have imposed a constant surface tension of γ_S = 120 mJ m^{-2}, according to our previous work (Miles et al., 2022). Note that at 328.15 K, the bilayer is in a liquid crystalline phase. Following this equilibration, the systems were quenched from 328.15 K to 300 K at a rate of 2.25 K ns^{-1} under constant (ambient) pressure and imposed surface tension (120 mJ m^{-2}). The systems were subsequently equilibrated at 300 K, where the bilayer is in the gel phase, via a 20 ns run. Once equilibrated at 300 K, extended MD runs of 3 μs were performed in the NVT ensemble, where the volume was chosen as the equilibrated average volume from the previous NPT simulations.

2.2.2 Thermogravimetric analysis

The raw materials' thermal stability and suitability for use in the twin-screw extrusion process were measured using a TGA (TA instruments, Leatherhead, UK) and analyzed using a TA instrument universal analysis 2000 software. Decomposition was deemed significant if weight loss over 5% occurred, where the onset of decomposition was determined using extrapolated tangents of slopes before and after degradation began. Thermal scans were performed from

0 – 400°C at 20°C/min, with the remaining weight plotted as a temperature function (n=3). Nitrogen was used as a purge gas throughout (flow rate sample: 60 mL/min, flow rate balance: 40 mL/min). All measurements were carried out in triplicates.

2.2.3 Melting point depression studies

Melting point depression studies were conducted on binary physical mixtures in a DSC 8000 differential scanning calorimeter (Perkin-Elmer, Windsor, Berkshire, UK). In a typical binary physical mixture preparation, approximately 500 mg samples were prepared at a 70% w/w drug loading before milling them for 8 min at 20 Hz in a ball mill (MM200, Copley Scientific Limited, Nottingham, UK). The DSC instrument was calibrated at the respective heat rates with indium and zinc for both melting point and heat of fusion. Nitrogen was used as a purge gas (flow rate: 40 mL/min) to maintain an inert atmosphere. 5 – 10 mg of sample was accurately weighed into aluminium pans and crimped using an aluminium pan lid. The pan was then subject to a thermal ramp at 5°C/min from 0 to 170°C. Plots of heat flow versus temperature were recorded and analyzed using Pyris software. The melting endpoint (T_{end}) was calculated at the intersection of the falling edge of the melting endotherms and the post-melting baseline. The peak maximum was taken to detect the lipid transition temperature. All measurements were carried out in triplicates.

2.2.4 Flory-Huggins thermodynamic modelling

Calculation of drug-lipid phase diagrams was performed using DSC analysis. Melting point depression studies across a range of drug loadings (90 to 50% w/w) for each drug (NPX and FEL) in a physical mixture with HSPC were carried out, and the end melting point was recorded as representing the complete melting of all crystalline drug within the sample. The melting depression data were then fitted by Flory-Huggins modelling, as previously established in our group (Tian et al., 2013). Drug lipid mixtures were prepared and measured using DSC, as described above. The fractions of molecular volume for drug-phospholipid systems were calculated from the ratios of the drug (NPX or FEL) over the selected phospholipids.

2.2.5 Powder X-ray diffraction

Powder X-ray diffraction (PXRD) was used to examine the degree of crystallinity in raw materials, physical mixtures, and melts to allow the evaluation of phase diagrams and the system's stability. Samples were analyzed at room temperature using a MiniFlex II Desktop Powder X-ray Diffractometer (Rigaku Corporation, Kent, England) equipped with Cu Kβ radiation, at a voltage of 30 kV and a current of 15 mA. Samples were placed onto a glass to-loading sample holder with 0.2 mm depression. All samples were scanned from 3 – 90 2θ in

continuous mode with a sample width of 0.03° and a scan speed of 2.0 °/min. Diffraction patterns were analyzed using PDXL software.

2.2.6 Preparation of felodipine and naproxen loaded liposomes

The twin-screw extrusion (TSE) method prepared drug-loaded and blank liposomal nanoparticles using optimized processes previously published (Andrews et al., 2023; Jacobs et al., 2022). Briefly, FEL, NPX, HSPC, and cholesterol at the relevant ratios were first ground by mortar and pestle and then mixed with xylitol as a hydrophilic carrier at a drug-phospholipid to xylitol ratio of 1:9 w/w. The premixture was fed into the TSE (Rondol Technology Ltd., France) and processed between 50 to 105°C. The screw configuration was composed of 90°/60° kneading and conveying elements for breaking down the particle size and dispersing liposomal nanoparticles. All the samples produced in this study were carried out in multiple repeats (≥ 3).

2.2.7 Lipid/liposome structural information

Small-angle X-ray scattering (SAXS) experiments were carried out using a Ganesha 300XL system (Xenocs, France). The instrument is automated with a movable detector inside the vacuum chamber and configured as a two-pinhole system with a high-brilliance micro-focus Copper source. The scattered X-ray photons were collected by a Pilatus 300K Solid-State Photon-Counting Detector with a pixel size of 172 µm. The scattering data obtained were radially averaged and normalized to the exposure time using SAXSGUI software. The obtained 1D spectra were processed as a function of the scattering vector $q = 4\pi\sin(\theta)/\lambda$, where 2θ is the scattering angle, and λ is the wavelength of Cu Kα = 0.154 nm. Silver behenate was used to validate the q calibration. The powder samples were loaded into 1.5 mm diameter borosilicate glass capillaries and sealed by a glue gun before the data collection at 30°C with an exposure time of 180 seconds. Multiple runs were carried out for each formulation.

2.2.8 Transmission light microscopy

Transmission electron microscopy (TEM, JEOL JEM-1400 series, Massachusetts, USA) and Cryogenic transmission electron microscopy (Cryo-TEM, FEI, Thermo Fisher Scientific, Eindhoven, The Netherlands) were both used to characterize the nanoparticles within the solid matrix and after reconstitution in water. For assessing the liposomal nanoparticle suspension within the solid polyol, the sample was slightly softened in a temperature-controlled oven (MN305, Genlab, Widnes, UK), a carbon-coated Copper grid (200 mesh, Agar Scientific, Stansted Essex, United Kingdom) was placed in the molten sample, followed by the sandwich of two glass coverslips. Once it was cold, the glass coverslips were separated and left with the solid sample on the copper grid. For assessing the liposome nanoparticles within the aqueous medium, the solid extrudates were dispersed within deionized (DI) water, then 3 µL

of the diluted sample was pipetted onto a previously glow discharged, lacey carbon film EM grid, blotted for 1.2 s and plunge frozen into liquid ethane using a Leica GP plunge freezer (Leica Microsystems, Wetzlar, Germany). The sample was kept at liquid nitrogen temperature while transferred to a Gatan 626 Cryotransfer holder (Gatan, Pleasanton, CA, USA) and imaged using TEM. Using low-dose acquisition software, images were acquired on a CETA camera (FEI, Thermo Fisher Scientific, Eindhoven, The Netherlands). A minimum of five microphotographs were collected from each sample.

2.2.9 Dynamic light scattering

Liposome particle size and size distribution were measured (in triplicate at 25°C) using a Nanobrook Omni (Brookhaven Instruments, USA). Samples were reconstituted and diluted to an HSPC concentration of 20 μg/mL using ultra-purified water, and the mean effective diameter (nm) and polydispersity were reported.

2.2.10 UV-Visible light spectroscopy

NPX was quantified using an ultraviolet/visible light (UV/vis) spectrometer (Cary 50, Agilent Technologies, California, US). The standards were prepared using 90% methanol and 10% water between the concentration range of 0.5 – 2.5 μg/mL for NPX and 2.5 – 20 μg/mL for FEL. All the standards were prepared in triplicate.

2.2.8 High-performance liquid chromatography

Quantification of FEL was carried out using an Agilent (California, US) 1260 infinity Quaternary system HPLC with a Kinetex 5u C18 100A, 150 x 4.6 mm column (Phenomenex, California, US) at 25°C. UV detection was used with a mobile phase of 10% water with 0.1% trifluoroacetic acid (TFA) and 90% methanol. The injection volume was set to 20 μL and a flow rate of 1 mL/min was used. A standard calibration was then prepared between the 0.5 – 100 (g/mL concentration range, allowing the drug concentration to be determined.

Quantification of HSPC was carried out using an Agilent (California, US) 1260 infinity Quaternary system HPLC with a Kinetex 5u C18 100A, 150 x 4.6 mm column (Phenomenex, California, US) at 45°C. A 1260 infinity II evaporative light scattering detector (ELSD) was equipped with a mobile phase of 5% water with 0.1% TFA and 95% methanol with 0.1% TFA. The injection volume was set to 20 µL, and a 2 mL/min flow rate was used. A standard calibration was prepared between the 30 - 100 (µg/mL concentration range) for HSPC quantifications. The limit of detection and quantification were calculated to be 17.4 and 52.7 µg/mL, respectively. The accuracy and precision of the method are summarised in Table S2.

2.2.9 Encapsulation Efficiency (EE)

The EE was determined using centrifugal filters (Merck, Millipore, USA) with a 10 kD filter to separate the free and encapsulated drugs. Formulations were dispersed in Millipore water to produce a stock with a 10 µg/mL drug concentration. 500 µL aliquots of the stock were transferred to each centrifuge filter tube and spun for 20 min at 10,000 rpm at 4°C. This ensured adequate supernatant recovery without the risk of liposome rupture. The supernatant was then diluted to an acceptable concentration. The solution was analyzed using a Cary 60 UV/vis spectrometer (Agilent Technologies, USA) at 232 nm for free drug content, compared to the calibration curve as described. The total drug concentration was found by diluting 1 mL of stock solution to 10 mL with methanol and sonicating for 30 min. The solution was then analyzed by UV-vis to determine the total drug content. The EE could then be calculated based on the free drug content over the total drug content of the liposomal nanoformulations after reconstitution in aqueous media.

To validate the method, the entrapped drug contents in select formulations were also measured following the centrifugation, as described above. The filter insert was removed and inserted upside down into a clean Eppendorf tube before being centrifuged for 4 mins at 10,000 rpm to extract the liposomes from the filter. The liposome was redispersed in the PBS buffer, aliquoted, and dissolved in methanol to an appropriate concentration for quantification. The total drug content of the processed formulation was also quantified by dissolving the entire formulation within an organic solvent. Similar procedures were employed for FEL formulations except a 0.5% sodium laureth sulphate (SLS) in the aqueous medium to solubilize the FEL for complete detection.

2.2.10 Drug release

Membrane dialysis was used to determine the release profile of drugs from the liposomal formulations. The solid formulations were dispersed to a suitable volume of medium, ensuring the maximum theoretical concentration was reached, 5 µg/mL for NPX (in PBS pH=7) and 20 µg/mL for FEL (PBS pH 7 and 0.5% SLS in PBS pH=7). 5 mL of the liposomal suspension was immediately pipetted into a dialysis tubing cellulose membrane (molecular weight cutoff 14K, Sigma-Aldrich, Gillingham, UK) and pre-soaked in the release media overnight. The dialysis bag was sealed with clips before being placed into 50 mL of the release media at 37°C. This was then placed into an incubator shaker at 37°C and 40 rpm for the experiment. At designated time points, a 2 mL aliquot was withdrawn and replaced with a release medium. At the end of the experiment, the bag was burst into the media, and the final total drug concentration was quantified. As a comparison, the centrifugation-based drug release method was employed. The liposomal formulations were dispersed as previously described, divided equally into several small vials, and placed in an incubator shaker at 37°C and 40 rpm. At the

designated time points, the small vials were centrifuged at 10,000 rpm for 20 min at 4°C. The supernatant was then collected for drug quantification.

2.2.11 Statistical Analysis

All data were examined with a significance level of $p < 0.05$. The effects of ball millings on the T_{end} of the drug's melting points and the dissolution data were further analyzed using a one-way ANOVA using crystalline NPX as the control to determine significant differences between various liposomal formulations, as well as using a post-hoc test to compare with each formulation to determine the effect of altering factors.

3. Results and Discussion

3.1 Atomistic understanding of the FEL/NPX - HSPC bilayer interactions

3.1.1 Computational setup

A pure 1,2-distearoyl-sn-glycero-3-phosphocholine (DSPC) lipid bilayer system was constructed using CHARMM-GUI, with 30 lipids per leaflet (60 per system). Six DSPC molecules were manually edited, removing two carbon atoms from the primary lipid tail to create HSPC lipids (the relevant force field parameters have also been modified accordingly). Initial equilibration MD runs were carried out at 328.15 K. Following equilibration in the liquid crystalline phase, the system was quenched to 300 K and equilibrated within the gel phase. Once equilibrated and quenched, the simulation box's in-plane dimensions were 3.89 x 3.89 nm. The details of this computational approach can be found in the Methods section. NPX and FEL molecules (one molecule of either species per simulation box) were initially solvated in TIP4P/Ice water within a 3.2 nm cubic box. In these simulations, NPX was simulated in its de-protonated form (the pKa of NPX is ~ 4.15, which means that its carboxylic group will be mostly de-protonated at physiological pH) (Li and Cooper, 2012). These systems were then merged with the equilibrated HSPC systems. A representative snapshot of the whole computational setup, containing the HSPC bilayer and one FEL molecule, is shown in Figure 1. We remark that whilst the actual liposome nanoparticles are curved objects, a ~4 nm section (such as the one we considered in our MD simulations) of these systems can be considered entirely flat.

3.1.2 Umbrella sampling

To investigate the energetics of the insertion/release of either FEL or NPX molecules in/from HSPC bilayers, we have utilized the umbrella sampling (US) enhanced sampling method (Torrie and Valleau, 1977, 1974). US is a computational technique employed to estimate the free energy landscape of a system/process. It involves performing simulations at various points along a "collective variable" (CV), i.e., a mathematical object that allows us to distinguish the system's different states and obtain a free energy profile relative to the process

we are interested in (Bhakat, 2022). In this case, we have selected as our collective variable the z-component of the distance d between the centre of mass (COM) of the drug molecule and the centre of mass of the HSPC bilayer:

$$d_z = \mathrm{COM(drug)}_z - \mathrm{COM(bilayer)}_z. \qquad \text{Equation 1}$$

We perform restrained MD simulations for different points along this CV using a biased potential, or "umbrella," to enhance sampling (particularly in energetically unfavourable regions). Each umbrella typically consists of a harmonic potential characterized by a spring constant, *k*, which quantifies the strength of the bias applied to keep the system around a given CV value. The spring constant is crucial for controlling the extent of fluctuations around this point, affecting both the efficiency and accuracy of the sampling.

By combining data from these biased simulations through a reweighting process, such as the weighted histogram analysis method (WHAM), it is possible to reconstruct the unbiased free energy profile along the reaction coordinate (Hub et al., 2010). Umbrella sampling is particularly useful for studying processes with high (i.e., higher than the thermal energy at the temperature of interest) energy barriers that are difficult to sample adequately through straightforward molecular dynamics simulations. US is a free energy-based enhanced sampling method that is especially suited to the problem at hand, given that we know the initial and final states of the process we are interested in. Specifically, our initial state corresponds to the situation where the FEL or NPX molecule is in the water phase above the HSPC bilayer, and our final state corresponds to the situation where the FEL or NPX molecule is in the water phase below the HSPC bilayer. Thus, we aim to determine the free energy changes associated with the drug molecules percolating through the HSPC bilayer.

An initial simulation was run with the location of the bias moving along the selected CV by 1 Å every 10-50 ns (depending on the drug molecule and its position relative to the lipid bilayer); i.e. a 10-50 ns run with the bias centred at d_z = +40 Å, a 5 ns run with the bias centred at d_z = +39 Å and so on up until d_z = −40 Å. The bias applied was a harmonic potential, with a spring constant of k = 2000 kJ mol^{-1}. This choice in terms of the spring constant allowed us to overcome the relevant free energy barriers whilst still resulting in a substantial overlap between the different umbrellas (see the top two panels of Figures 2a and 2b). "Walls" (i.e. additional potentials aimed at preventing the molecules from crossing specific boundaries within the system) at d_z = ±45 Å were introduced to keep the FEL/NPX molecule in the relevant region of the system. The WHAM code written by Grossfield was used to compute the free energy landscapes with respect to the CV d_z (Grossfield, 2022), with a bin width of 0.2 Å. The results of the US simulations for both NPX and FEL are summarised in Figure 2.

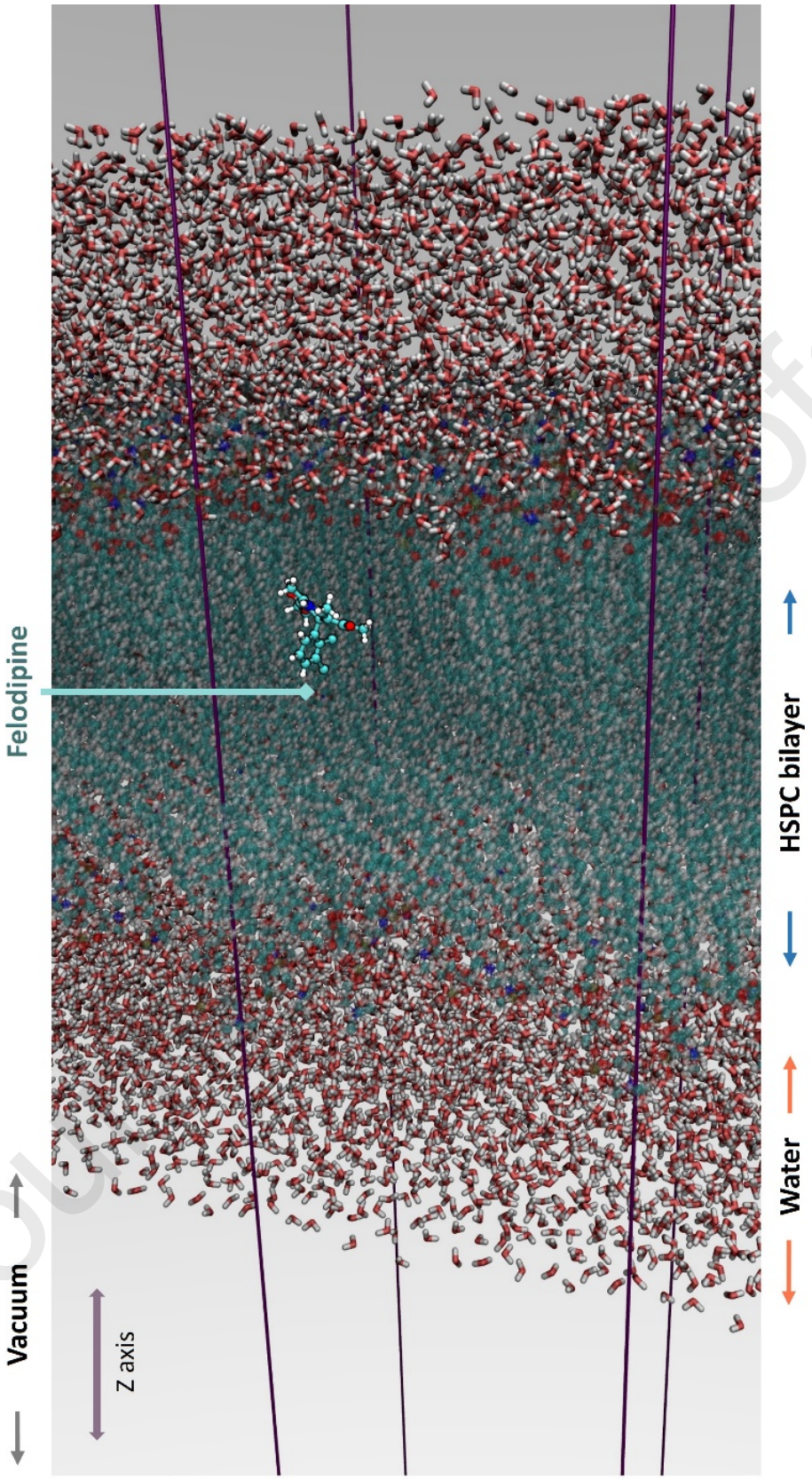

Figure 1. Schematics of the computational setup. A felodipine molecule is driven (by means of enhanced sampling simulations) from the water phase (~ 3 nm thick) into the HSPC bilayer. The simulation box is depicted in purple. Note that the vacuum regions (only partially included in the Figure) extend for roughly three times the size of the system along the vertical (z) axis. The in-plane dimensions of the system are ~ 4 nm.

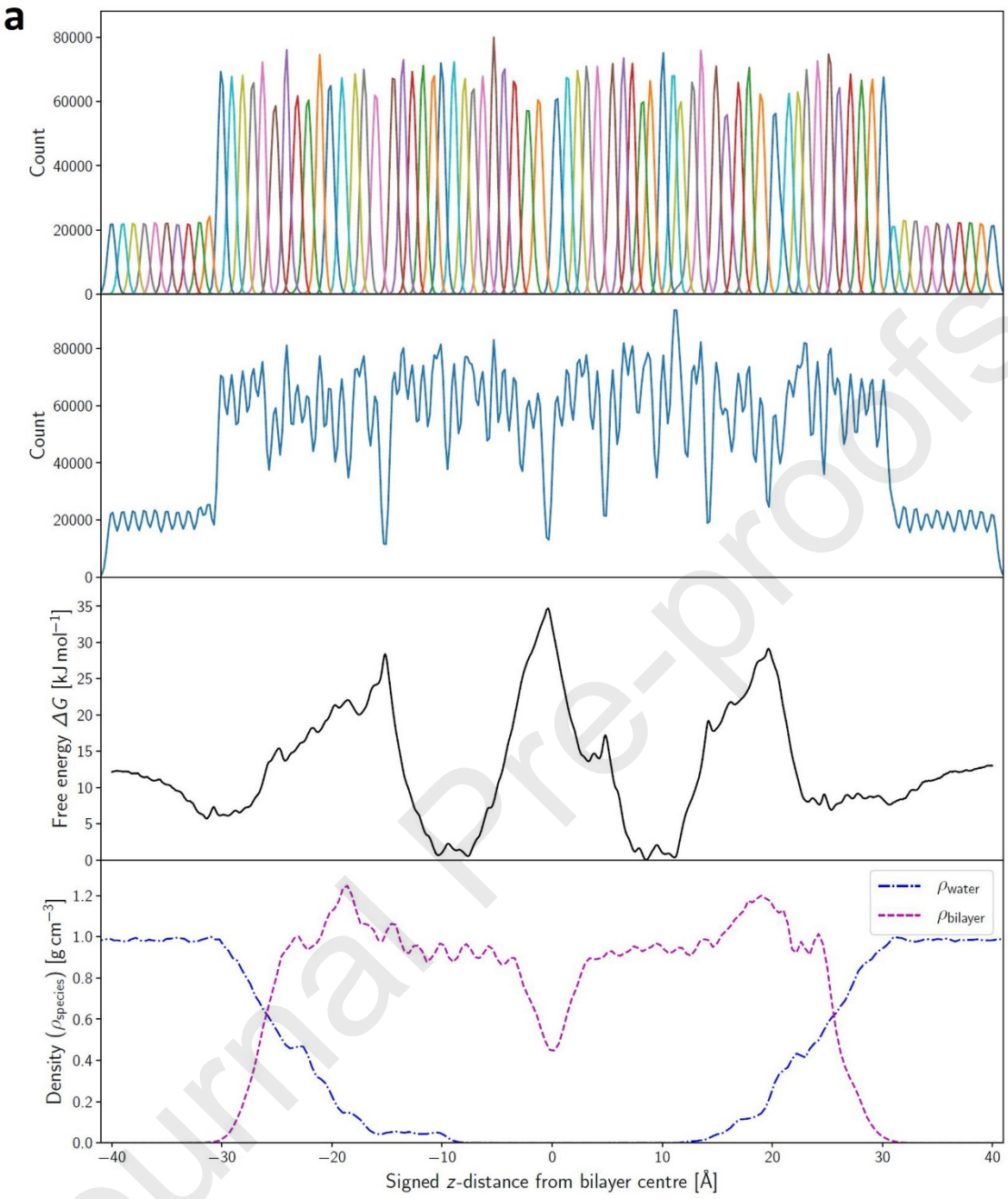

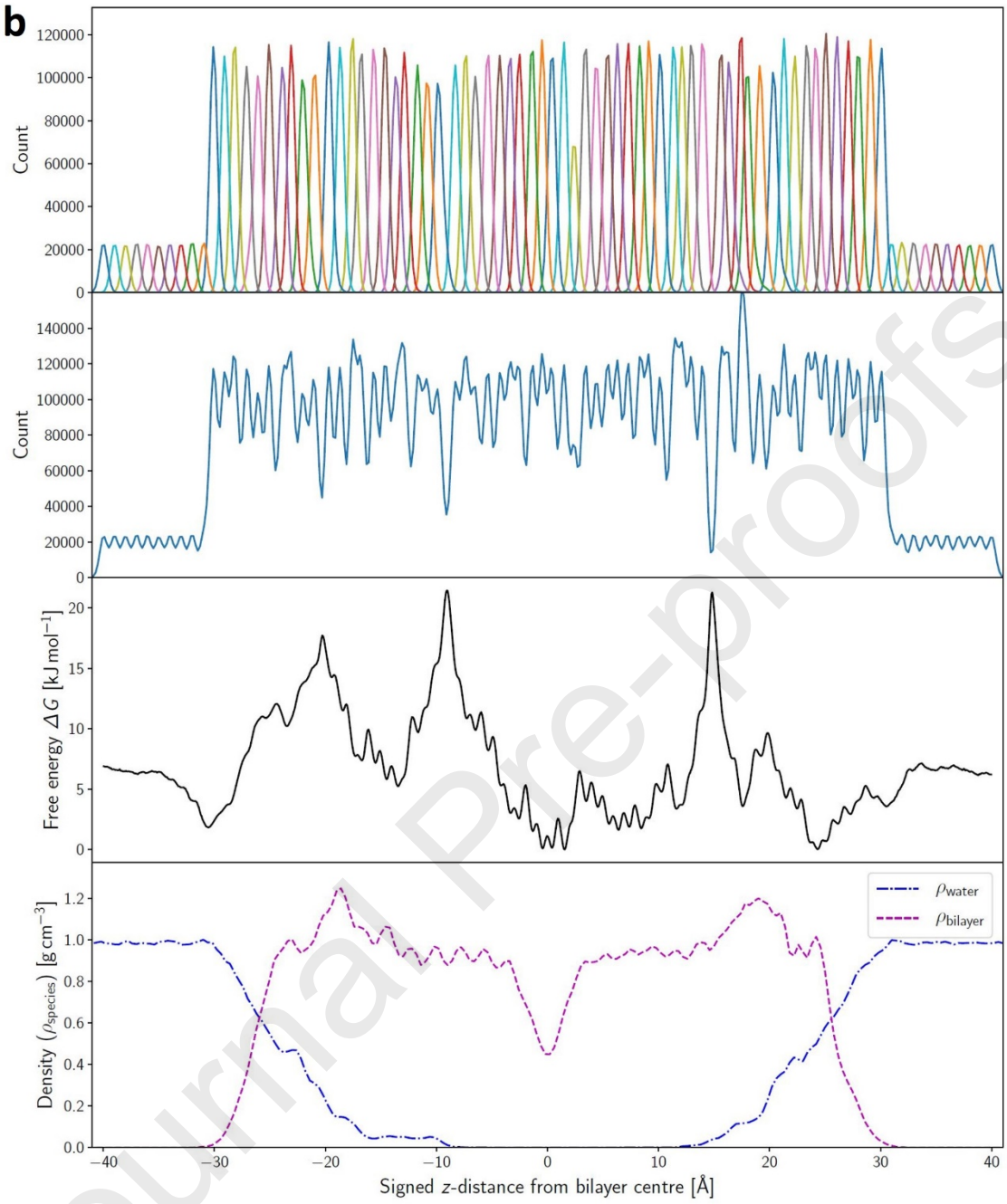

Figure 2. Results from umbrella sampling simulations of FEL-HSPC (a) and NPX-HSPC (b) bilayer systems. The top panel shows the histograms of the z-distribution of the drug molecule (with respect to the bilayer centre, as shown in Figure 1) for each simulation. The bins used for the histograms were equal to 0.2 °A width, from -45 °A to 45 °A. The second panel shows the sum of these histograms. The third panel shows the estimate for the free energy computed by the WHAM software. The fourth panel shows the bilayer and water density profiles to reference the other panels. The x-scale is the same for all panels.

The density profiles reported in the bottom panels of Figure 2a and Figure 2b indicate that the hydrated region extends up to 10 Å into the HSPC lipid bilayer. In the case of FEL, we argue that the drug molecule tends to sit within the HSPC bilayer, given the two local free energy

minima observed in correspondence with the HSPC hydrophobic lipid tails (d_z ~ +/- 10 Å). Note that these two minima are energetically favourable (by ~5-10 kJ/mol) with respect to the rather shallow energy minima observed for FEL at the water-lipid interface (d_z ~ +/- 30 Å). The percolation of the molecule through the hydrophilic headgroup region of the HSPC lipid bilayer (-25 Å < d_z < 10 Å) does require a substantial free energy barrier (~25 kJ/mol) to be overcome. Moreover, crossing the bilayer centre (d_z = 0 Å) requires an even higher free energy cost of ~35 kJ/mol.

Interestingly, compared to FEL, lower free energy barriers were observed for the NPX molecule as it crosses the HSPC bilayer – albeit we remark that the free energy profile we have obtained for this molecular species is not perfectly symmetric, which suggests some inhomogeneities within the HSPC bilayer. Nevertheless, NPX's local free energy minima at the interface between the bilayer and water (d_z ~ +/- 30 Å) are more energetically favoured than the local free energy minima for NPX observed in correspondence of the HSPC hydrophobic lipid tails (d_z ~ +/- 10 Å). This suggests that, in stark contrast with FEL, NPX tends to sit at the water-bilayer. As NPX moves towards the centre of the HSPC bilayer, a bi-modal free energy landscape was observed, suggesting that different molecular conformations are needed for NPX to cross specific regions of the HSPC bilayer. However, the average values of the free energy barrier are consistently lower than the FEL-HSPC system, suggesting better miscibility for the NPX-HSPC system, which is consistent with previous experimental evidence (Go and Ngiam, 1997). The relatively higher free energy barrier between FEL and HSPC suggests possibly limited miscibility of the drug-phospholipid combination in comparison with the NPX-HSPC system; if encapsulated within, a slow drug release of FEL out of the HSPC liposomal bilayers is expected. Thus, we argue that the atomistic understanding of the interactions between small molecule drugs and lipid bilayers could be of great interest to the nanocarrier design concerning the critical quality attributes of the final liposomal drug delivery system, such as the drug loading capacity, stability, and drug release kinetics (Barenholz, 2012; Rivnay et al., 2019; Stone et al., 2016).

3.2 Thermodynamic modelling of NPX and FEL with phospholipids

While the MD and US can provide atomistic level information for small molecule lipid bilayer systems, it is also crucial to recognize that only one or two drug molecules were involved in these simulations (< 1-3% weight ratio). However, a sustained higher drug loading is crucial for efficiently applying liposomal drug delivery vesicles. Depending on the system's thermodynamics and self-assembling characteristics, the potential drug loading within the liposomal vesicle can range from 10% to 30%, w/w (Akbarzadeh et al., 2013). At this scale, thermodynamic modelling can be instrumental in translating the atomistic findings to the design and realization of drug-encapsulated liposomal nanoformulations (Fearon and Stokes,

2017). Thermogravimetric analysis (TGA) was used to confirm that at temperatures lower than 200°C, less than 5% w/w weight loss occurred in any phospholipids (Table S1).

3.2.1 Melting depression studies

Depression in a drug's melting point suggests strong interaction between the components involved and was therefore used to predict miscibility between the drug and lipid excipients in this study (Baird and Taylor, 2012). The hypothesis was that increased miscibility, depicted by a depression in the drug melting point, would correspond to the potential for increased drug loading in a liposomal bilayer system. DSC was utilized to investigate the lipid candidates and their degree of interaction with the selected drugs (FEL and NPX). Physical mixtures of drug and lipid were prepared by ball milling, ensuring the mixtures' homogeneity. It also promoted interaction between components and converted some drugs to the amorphous form, which would cause a depression in melting point, not related to the mixing of drug and lipid. It was thus essential to determine the impact of ball milling time on the melting depression of the phospholipid-drug mixture. As shown in Figure 3, a milling time of 6 min was deemed optimal. No statistically significant difference was observed between the T_{end} after 6 min of milling according to unpaired t-tests that compared the melting depression after each milling period. The level of interaction between components and, therefore, the extent of melting point depression is impacted by several factors. Significantly, the level of homogeneity, particle size, composition and chemical interaction between the components. By optimizing the ball milling process, differences in melting point depression were limited to chemical interactions between components (Koch et al., 1989).

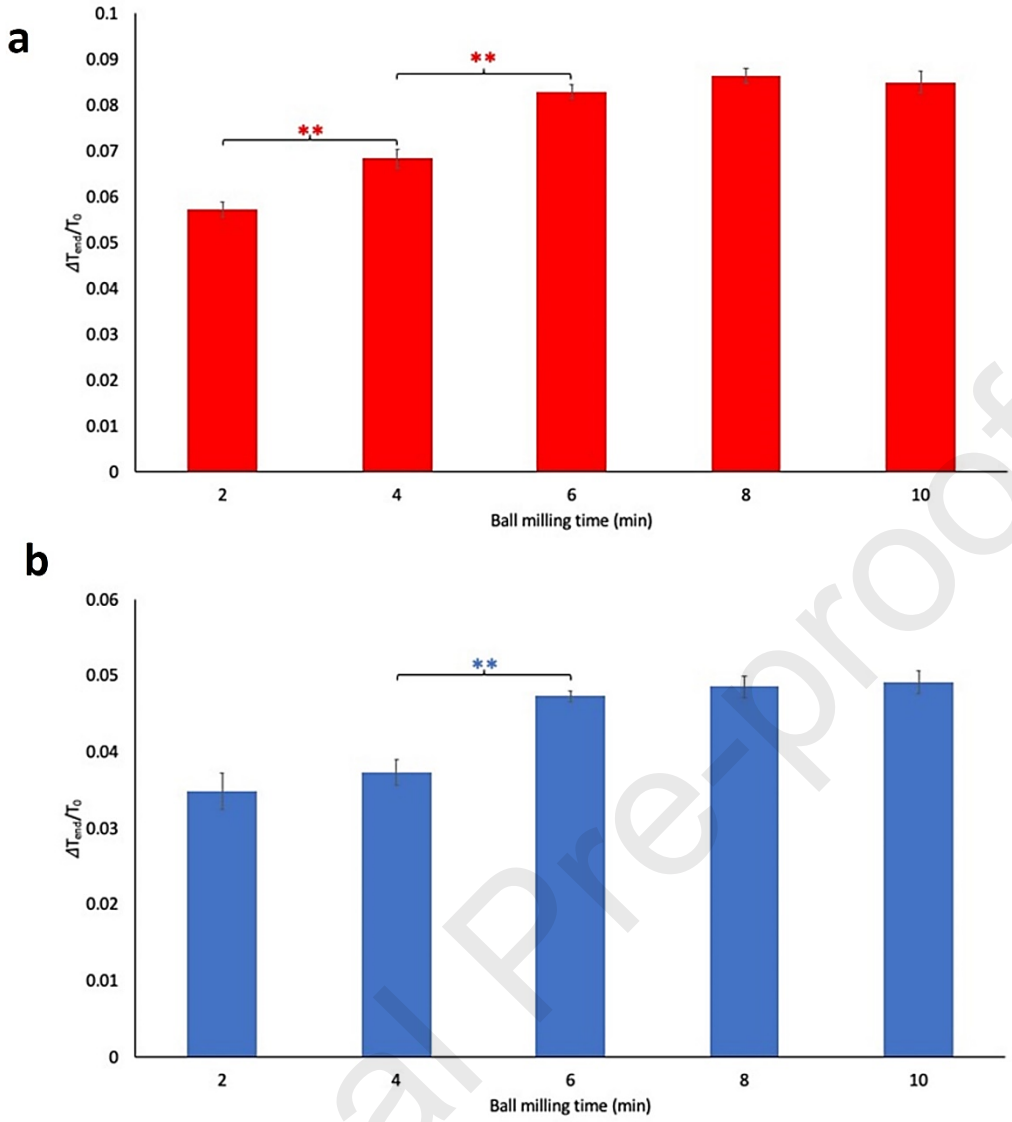

Figure 3. Impact of increasing milling time on the melting depression of a 70% w/w mixture of drugs with HSPC, (a) FEL-HSPC and (b) NPX-HSPC. The error bars represent the standard deviation (n = 3); unpaired t-test significance level results are displayed at each point.

As illustrated in Figure 3, milling time initially impacts the level of depression at the melting point until the homogeneity of the mixture is reached (Meng et al., 2015). After 6 minutes for FEL and NPX, there were no further significant differences in the melting depression as the balling milling time increased. The most common lipids used in the formulation of liposomes are PCs, comprising a hydrophilic phosphate head and a hydrophobic acyl tail with which lipophilic drugs will interact. The selection of a suitable phospholipid was carried out by investigating, via melting point depression, the impact of the acyl chain length of various phospholipids (HSPC (C16-18), DSPC (C18), DPPC (C16) and DMPC (C14)) on the miscibility with selected drugs (FEL and NPX) at a 70% w/w loading. Figure 4 demonstrates the difference in transition temperatures of each PC and the influences of the acyl chains. HSPC

and DSPC have their main transition at approximately 100°C, DPPC was 80 – 100°C and DMPC 60°C. Figure 2a showed a depression in the T_{end} of each phospholipid – drug mixture, indicating that a strong interaction occurred between the phospholipids and the two hydrophobic drugs. An endothermic peak in the 40 – 100 °C ranges was observed in each physical mixture, which was attributed to the phospholipid transition temperature (Eze, 1991). An endothermic peak in the 100 – 160 °C range was accredited to the melting points of the drug.

For each data set, the melting depressions were interpreted using a one-way ANOVA followed by a post-hoc Tukey test when significant differences were observed. Regarding FEL, significant differences between DSPC and DMPC were observed in the levels of melting depressions. For NPX, significant differences in melting depression were also observed, and the level of phospholipid – NPX interaction may be ranked as DMPC > DPPC > HSPC and DSPC. The results demonstrated that the choice of phospholipid impacted the melting depression and interactions between components. To avoid complications of this initial screening step, the selection of optimum milling parameters and DSC conditions was evaluated by a systematic approach using a method previously established (Donnelly et al., 2014). NPX showed a trend of more interaction with shorter acyl chains, and FEL revealed the highest melting depressions with DMPC and DSPC. It was reported that increased chain lengths can lead to improved encapsulation in liposomal formulations (Duangjit et al., 2014; Mohammed et al., 2004).

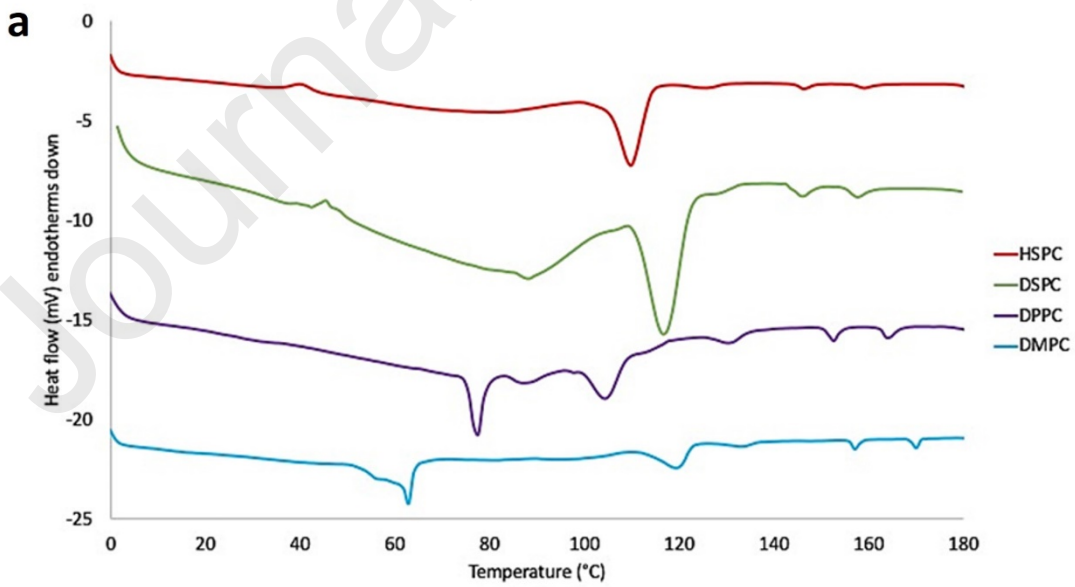

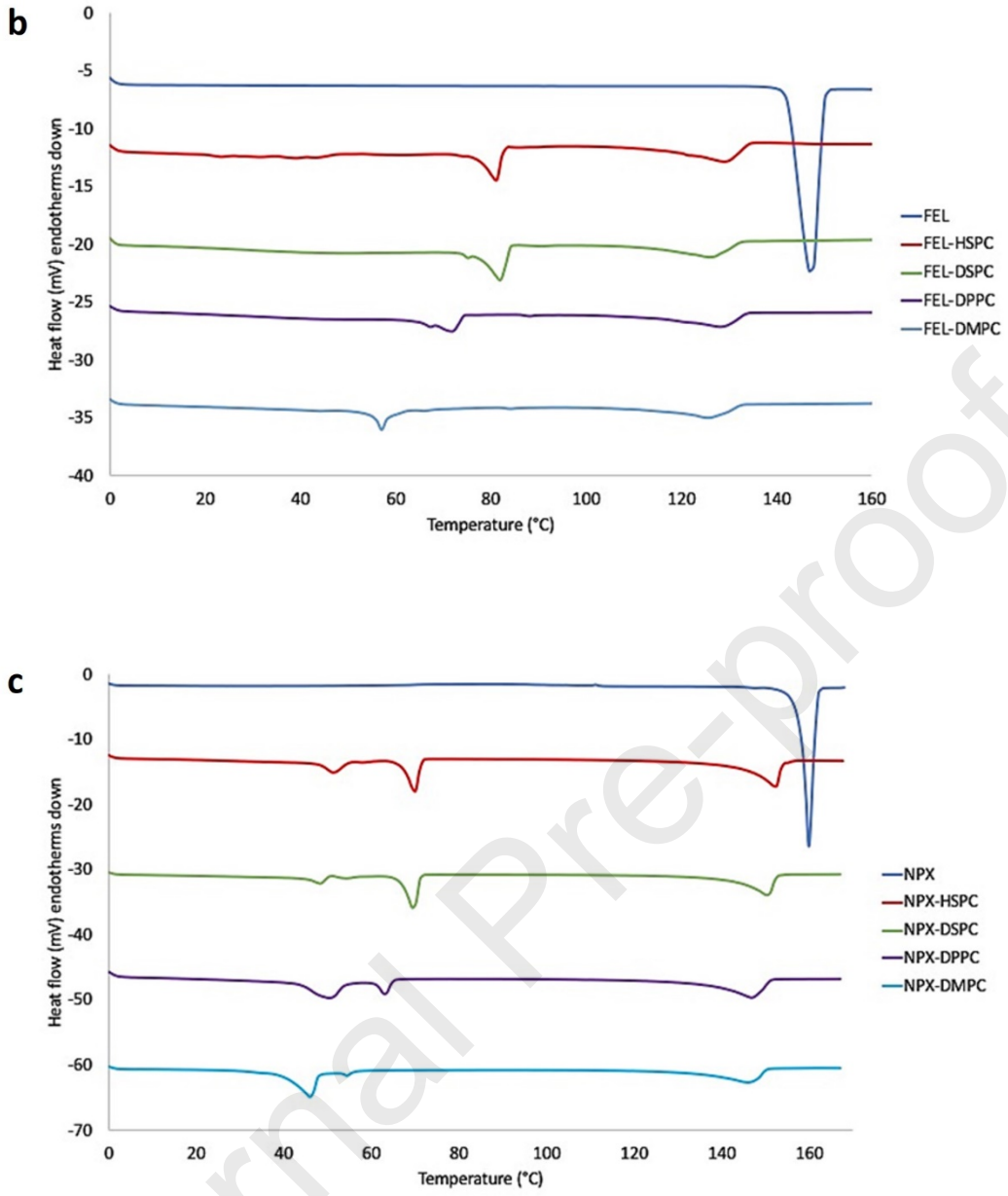

Figure 4 DSC thermograms of pure phosphatidylcholines, 20°C/min heating rate (a), 70% w/w FEL with various phospholipids, 5°C/min heating rate (b) and 70% w/w NPX with different phospholipids, 5°C/min heating rate (c)

However, Chang *et al.* demonstrated an increasing interaction of a hydrophobic drug with decreasing acyl chain lengths (Chang and Flanagan, 1995). In this experiment, both phospholipids and drugs were still in the solid state, where the surface interactions between the two components were the main driving force for melting depression. Indeed, the different phospholipid transition temperatures were observed when mixed with the two drugs. Regarding HSPC, the phase transition temperature was reduced from 100°C (pure form) to 80 and 60°C in the presence of FEL and NPX, respectively (Figure 4). It has been reported that incorporating hydrophobic drugs into the liposome has the impact of lowering the

transition temperature by disrupting the order of the acyl chains (Chang and Flanagan, 1995; El Maghraby et al., 2005). It may be postulated that NPX had a stronger interaction with HSPC than FEL from the solid state.

3.2.2 Flory-Huggins modelling

F-H thermodynamic modelling was used to estimate the level of miscibility between components over a temperature and composition range for drug-HSPC combinations (FEL and NPX). While we acknowledge that F-H modelling is limited to the non-specific interaction between the components, it can still provide a simplified approach to the composition-dependent miscibility between the drug and HSPC. This study uses this modelling to provide temperature-composition guidance to the anhydrous twin-screw extrusion process (Jacobs et al., 2022). In the DSC analysis, for each drug, an apparent depression in the pure drugs melting endotherm for both FEL and NPX systems was obtained (Figure S1). The data obtained from the melting depression studies indicate that both FEL and NPX would be miscible within the phospholipid HSPC at lower concentrations. An interaction plot was constructed to reveal the interaction between the drug molecules and HSPC where the system's miscibility at room temperature regions may be extrapolated (Figure 5). The gradient of the line detailed the nature of the system and the effect on miscibility when temperature is increased or decreased. The systems of FEL-HSPC displayed a positive gradient, which is characteristic of upper critical solution temperature (UCST) behaviour where miscibility will decrease in lower temperature regions. The trend line in the NPX-HSPC system demonstrated a lower critical solution temperature (LCST) behaviour indicated by a negative gradient, suggesting better miscibility at all temperatures (Tian et al., 2020).

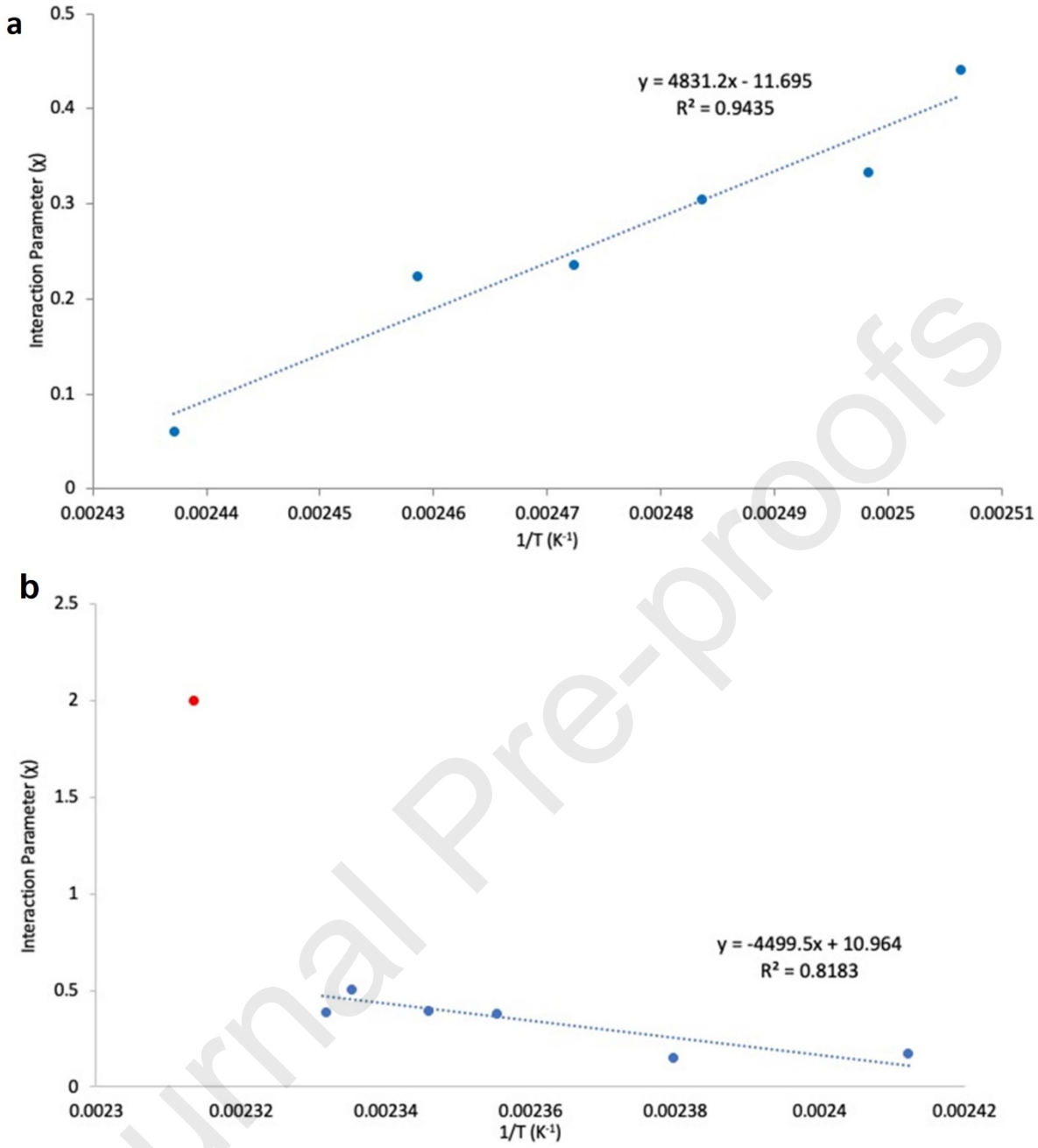

Figure 5 Least square regression fit of the calculated Flory-Huggins interaction parameter against 1/T from the T_{end} for (a) felodipine and (b) naproxen; the outlying points (red) were not included when performing linear regression.

With the F-H constants derived from linear regression, the phase diagrams for FEL-HSPC and NPX-HSPC were constructed (Figure 6). A change in the interaction parameter shifts the liquid-solid boundary of the drug-HSPC binary mixture. The boundary will move towards lower temperatures and higher weight fractions in more miscible systems. Above this liquid-solid line, the drug is expected to be fully miscible with the phospholipids. A spinodal line can be

plotted and depicts the point at which spinodal decomposition will occur; the shape indicates whether a UCST or LCST system is present (Ianiro et al., 2019).

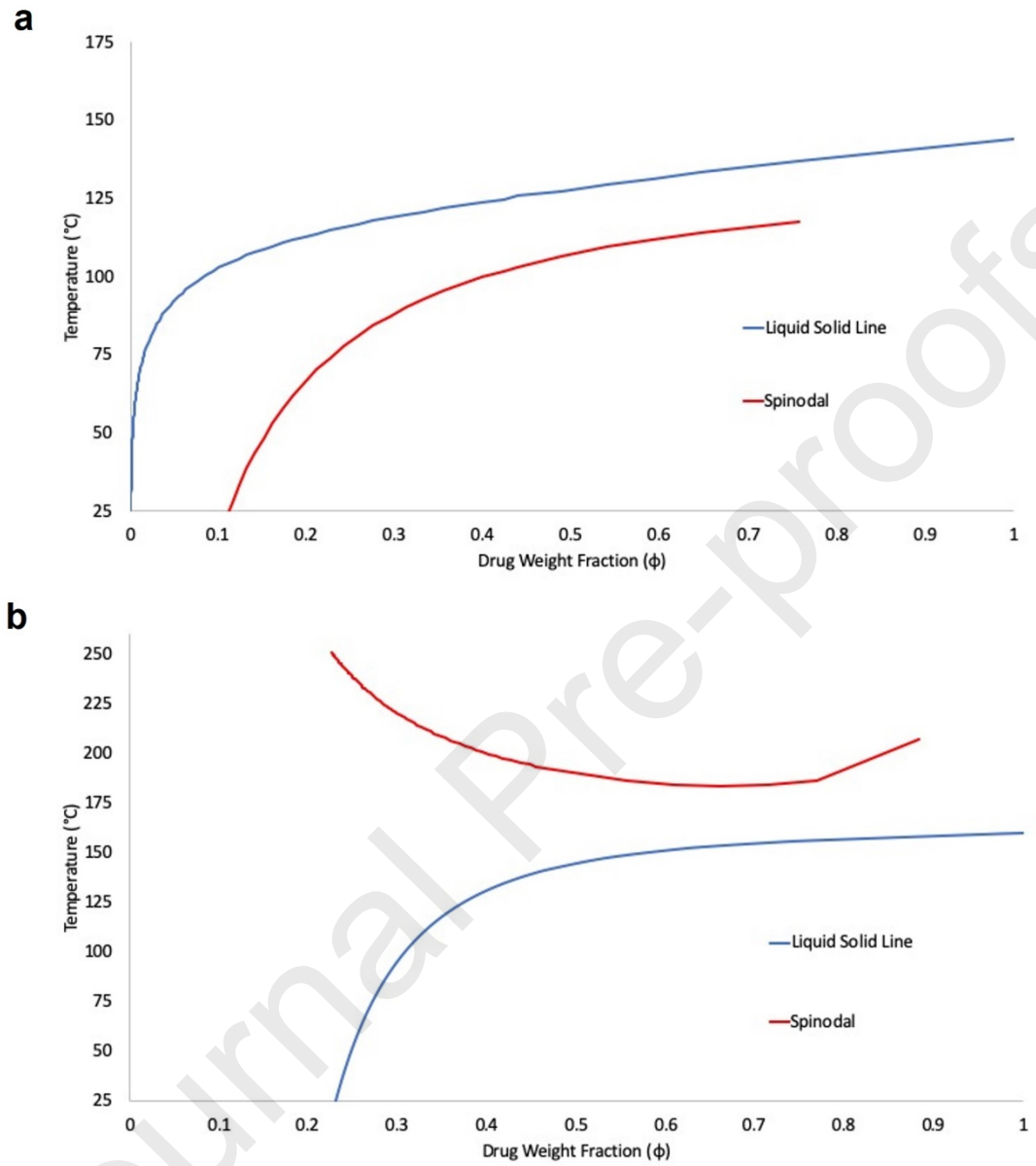

Figure 6 Phase diagram showing complete liquid-metastable-solid phase transitions for (a) FEL-HSPC with upper critical solution temperature (UCST) and (b) NPX-HSPC with a lower critical solution temperature (LCST)

Interestingly, the F-H model results show a similar trend to the outcomes obtained using molecular dynamic simulations, where better miscibility is expected from NPX-HSPC than from the FEL-HSPC system. From the simplified F-H approach, the maximum miscibility for NPX and FEL within HSPC is predicted to be approx. 23% v/v and 11% v/v, respectively (Niskanen and Tenhu, 2017). The construction of phase diagrams allowed the understanding of the phase behaviours of the drug-HSPC system based on the estimated miscibility at any

given temperature, which was used to guide the initial drug to HPSC loading of the formulations for the TSE process (Mehnert and Maeder, 2012; Shah et al., 2020).

Furthermore, with the F-H constants, the Gibbs free energy of mixing may also be obtained for the drug–HSPC systems (Figure 7). At the representative temperatures, a negative ΔG value indicated the high tendency for the small molecule drugs to be miscible with the phospholipids, while a positive value would depict a poor mixing capability. The shape of the Gibbs plot provided insight into the stability of the mixture. A concave shape suggests poor stability, and the system will be inclined to phase separate spontaneously. A convex shape indicated good mixing and formation of a stable single phase at the chosen temperature, and a sigmodal curve would show stability and homogeneity dependent on composition (Hengsawas Surasarang et al., 2017).

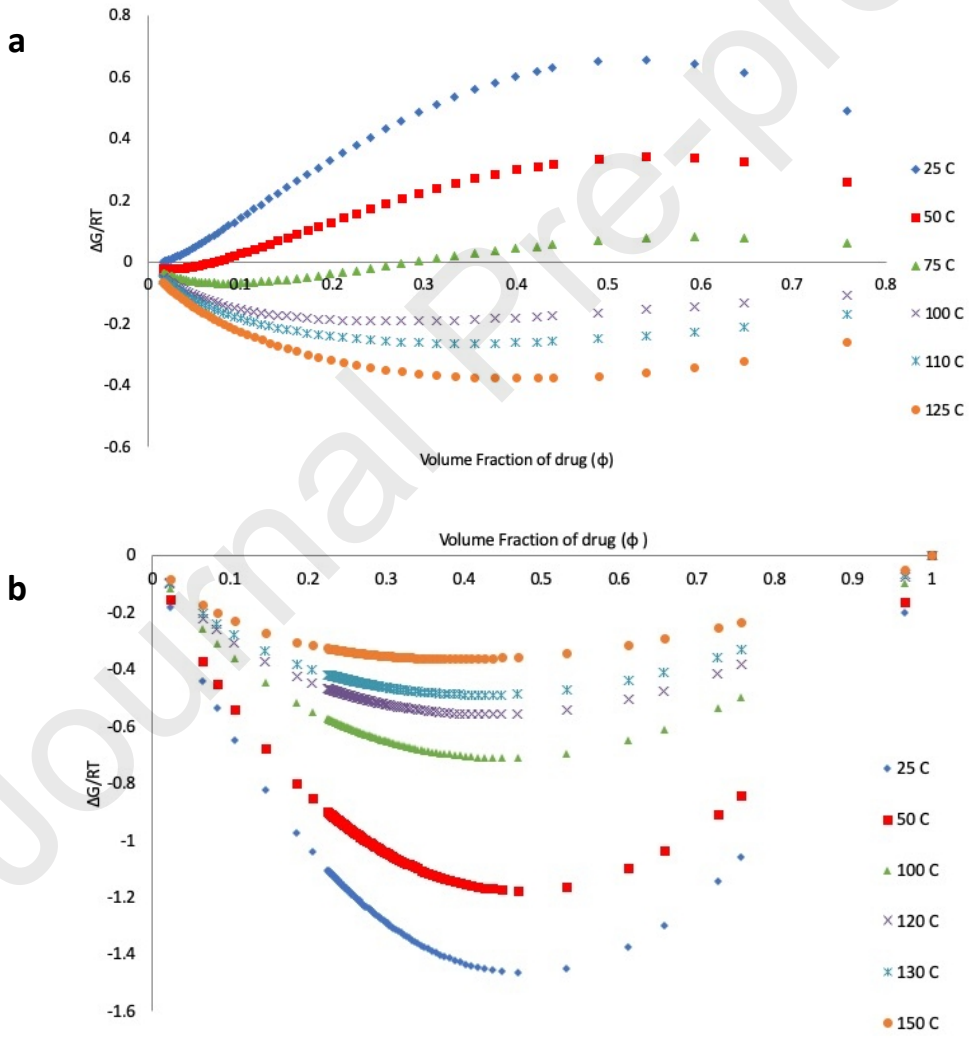

Figure 7 Gibbs free energy plot showing ΔG/RT against the volume fraction of drug in a drug-HSPC system between 25℃ and 150℃, for (a) felodipine and (b) naproxen.

FEL showed a concave curve shape for temperatures 100°C and above, while it demonstrated a convex shape below 75 °C. At 75°C, the curve had an intermediate sigmoidal shape. These results indicate that FEL may have enhanced miscibility with the HSPC when the temperature was above 100°C. At the same time, a low drug-HPSC loading is required between 75 - 100°C to ensure maximum miscibility. NPX demonstrated a concave shape throughout the temperature range investigated, indicating that encapsulation of the NPX within HSPC would be very likely once the kinetic barrier can be overcome, i.e. the phase transition of the HSPC (Mantsch and McElhaney, 1991).

3.2.3 Stability studies

PXRD and a polarised light microscope were used to characterize the drug-phospholipid mixtures and validate the predictions from the phase diagrams at several drug loadings (20, 50 and 80% w/w). A range of temperatures, 110°C to 150°C, representing various thermodynamic regions of the mixture were used for the sample preparation. The pure form of each drug showed several sharp diffraction peaks that were used to identify the presence of crystalline material in the binary mixtures, whilst the absence of these peaks would suggest the stability of the mixture. The most distinctive peaks were observed at 10° and 19° 2θ for FEL and NPX, respectively. HSPC showed a broad peak at 23° 2θ and did not interfere with the distinctive peaks of the drugs. The FEL-HSPC system closely agreed with the predictions from the phase diagram, with crystalline peaks in the diffractograms of the sample prepared with the drug at 80% w/w, 110°C and 130°C and at 50% w/w, 110°C. NPX-HSPC X-ray diffractograms were again in agreement with the predicted phase diagram, particularly at 20% w/w drug loading with the absence of crystalline peaks and good miscibility of the system. The data is summarised in Table 1, where a cross (X) represents the presence of crystalline peaks. After three months of storage at room temperature, samples were retested to determine if any change had occurred in the solid state, indicative of instability in the system. No changes were observed in the samples, indicating stability over the three months.

Most of the predictions from the phase diagram agreed with the validation samples, with the 20% FEL-HSPC (w/w) at 110°C was the only exception. In the phase diagram, it was located below the liquid-solid line, indicating poor miscibility between the two components during processing. However, experimentally, it was demonstrated to be amorphous in the diffractogram regions of the drug, suggesting an underestimation from the phase diagram prediction. Similar underestimation from the F-H modelling has been widely reported before, particularly considering the potential kinetic barriers of the phospholipid systems at room temperatures (Andrews et al., 2010).

Table 1. Summary of findings from PXRD of binary systems of drug and HSPC over three months, where X indicates the presence of the crystalline drug and ND noted for not detectable for crystalline drugs from both PXRD and polarised light microscope.

Drug	Felodipine						Naproxen					
Preparation Temperature (°C)	110			130			110			130		
Drug loading (% w/w)	20	50	80	20	50	80	20	50	80	20	50	80
Predicted	X	X	X	ND	ND	X	ND	X	X	ND	X	X
Day 1	ND	X	X	ND	ND	X	ND	X	X	ND	X	X
Day 30	ND	X	X	ND	ND	X	ND	X	X	ND	X	X
Day 90	ND	X	X	ND	ND	X	ND	X	X	ND	X	X

3.3 Preparation of the NPX and FEL liposomal formulations

With the two model drugs, NPX and FEL, solid extrudates containing drug-loaded liposomal were successfully manufactured via the one-step twin-screw extrusion (TSE) process (Jacobs et al., 2022). Compared to other scalable methods for producing drug-loaded liposomes, such as ethanol injection and thin film hydration, the one-step TSE process only uses the hydrophilic carrier as the process media. Implementing such a processing interface provides a highly efficient and scalable approach to producing liposomal nanoformulations, where the molten polyols act as the hydrophilic medium for the hydration and self-assembly of the liposomes (Dave et al., 2007). Postproduction, the solid sugar alcohol matrix with embedded liposomal formulations was obtained. Liposomal nanoparticles were obtained immediately after reconstitution in the aqueous media with structural information characterized using polarised light microscopy (support information, Figure S4), cryo-EM and SAXS (Figure 8 and Figure S5). The processing interface and ratios between phospholipids, drugs and cholesterol were critical to the drug release and stability of the liposomes (Li et al., 2014; Sultana and Sailaja, 2017). Similar to the NPX liposomal formulation, the scalable production method for FEL-loaded liposomes was also investigated (Boddu et al., 2017; Kassem et al., 2018). Following liposome production, comprehensive characterizations were carried out on the liposomal nanoformulation containing NPX and FEL; the results are summarised in Table 2. Examples of the SAXS profiles from blank liposomes and NPX or FEL-loaded HSPC liposomes in the sugar alcohol solids are summarised in Figure 8c. A sharp step was recorded for blank HSPC liposomes at q = 0.072 $Å^{-1,}$ indicating the possible inner lamellar spacing of d = 72 Å without loading any small molecule drugs (Bandara et al., 2020). This d value represents the lipid bilayer spacing in the nanodomains and is calculated from the scattering vector d = 2π/q. After

loading the NPX and FEL, clear differences were observed between liposomal nanoparticles. In the NPX HSPC liposomal nanoparticle, a sharp first-order lamellar peak q = 0.08 $Å^{-1}$ was recorded repeatedly, representing an inner lamellar spacing of d = 80 Å for NPX liposomal nanoparticles arrested within the sugar alcohol solid matrix. In addition, the appearance of the second-order peak L2 suggests a long-range lamellar structure formed within the NPX samples and many locally ordered structures (liposomal bilayers), which may contribute to the larger hydrodynamic diameters (Table 2). The interplanar distance of 80 Å agrees with the scale of MD simulations (Figure 2). In comparison, the sharp peak in the FEL HSPC liposomal nanoparticles was recorded at q = 0.07 $Å^{-1}$, revealing the closer packing of the bilayer structure compared to the blank or NPX-loaded liposomes. The SAXS results agree with the thermal analysis and cryo-EM evaluations, where the mixture of unilamellar and multiplayer structures are observed for both NPX and FEL liposomal nanoparticles after the TSE process (Figure 2 b&c). The size of the NPX and FEL liposomal nanoparticles calculated from SAXS data is not performed in this study due to the q-range limitations. The Ginner region must be observed below the measuring range judging from the size of NPX and FEL liposomes of ~ 200 nm (the Ginner region for this size is q < 0.002 A^{-1}).

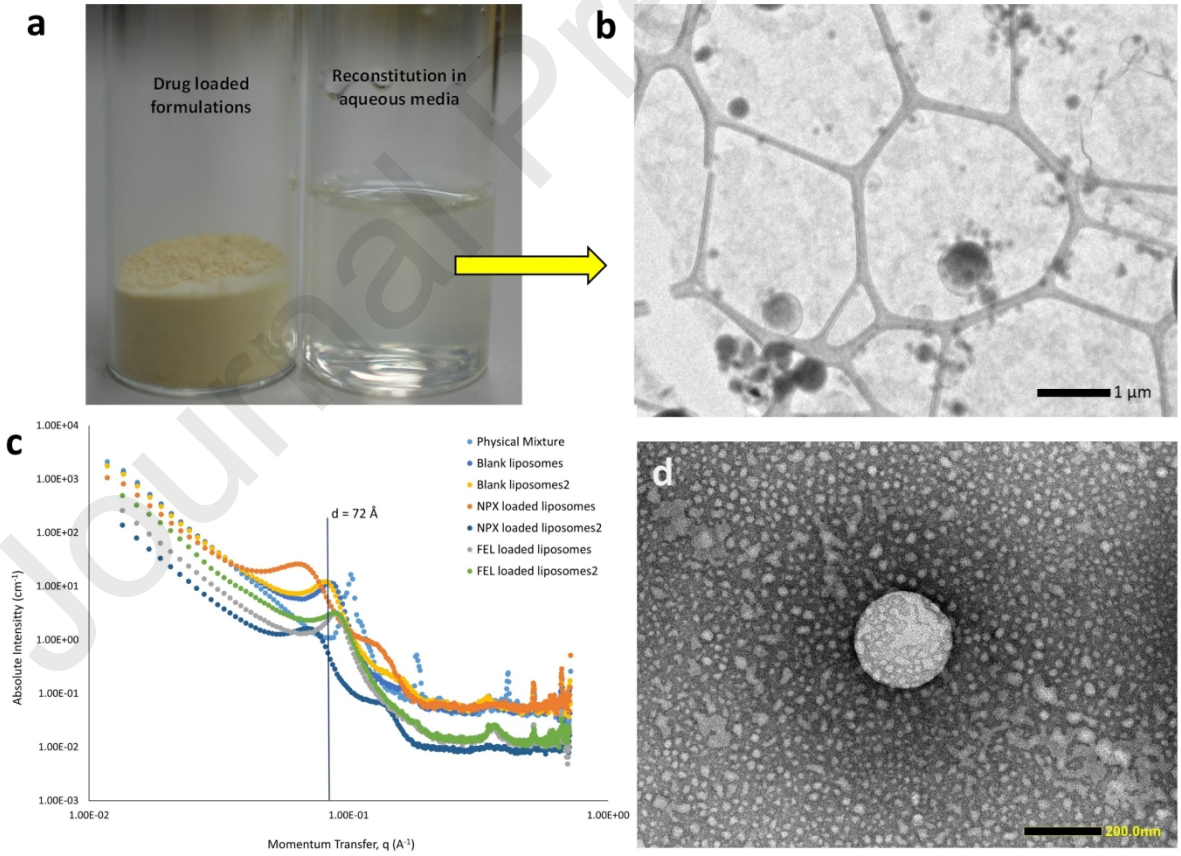

Figure 8 The resulting liposome containing sugar alcohol solid matrix (a); the liposomes after reconstitution in aqueous media and characterized by CryoEM (b) and SEM (d), and small angle X-ray

scattering of the sugar alcohol solid matrix at room temperature; the scale bars represent 1 μm in (b) and 200 nm in (d).

Corresponding to the SAXS results, uniform liposomal formulations with particle sizes ranging from 170 to 250 nm were obtained for both NPX and FEL formulations after reconstitution in aqueous media (DLS). FEL formulations are generally smaller in particle size and higher in drug encapsulation efficiency than the NPX formulations, irrespective of the HSPC and cholesterol compositions. The larger particle size of the NPX formulation agrees with molecular modelling, perhaps due to a small portion of NPX residing at the water-phospholipid interface rather than the inner space of the liposomal bilayers. As predicted by the MD and US, the local free energy minima for the NPX-HPSC system were identified at ± 30 °A from the bilayer centre. In contrast, FEL prefers to be complexed with the hydrophobic tails with local free energy minima at ± 10°A from the bilayer centre (Cárdenas et al., 2023).

Further to the investigations, eight liposomal formulations were selected for drug release studies: NPX1-4 denoted naproxen and FEL1-4 denoted FEL at different compositions. The final phospholipid concentrations after reconstitution for the selected liposomal formulations are summarised in Table 2. The responsible molar ratios of HSPC in NPX formulations were investigated in the range of 53 to 75%, with cholesterol (CHOL) ranging from 7.5 to 30% and NPX from 12 to 31%. By varying these compositions, the impacts of the HSPC and cholesterol compositions may be investigated, and these results are used to validate our understanding of the molecular dynamic and thermodynamic modelling.

Table 2. Summary of characterization results for naproxen and felodipine formulations; results are presented in average values ± standard deviation, n=3); the molar compositions for HSPC, CHOL and drug in the reconstituted liposomal formulations

NPX	Z-average Particle Size (nm)	PDI	Drug recovery (%)	EE (%)	HSPC molar (M/M) %	CHOL molar (M/M) %	Drug molar (M/M) %
NPX1	202.9 ± 4.8	0.34 ± 0.07	99.2 ± 0.6	88.1 ± 0.7	62	18	20
NPX2	203.0 ± 5.1	0.19 ± 0.03	89.7 ± 0.1	71.3 ± 3.6	56	30	14.1
NPX3	213.4 ± 3.5	0.28 ± 0.02	104 ± 1.3	73.8 ± 0.1	75.7	7.5	16.9
NPX4	229.8 ± 4.2	0.23 ± 0.04	97.1 ± 0.8	70.0 ± 2.1	56	15.2	28.8
FEL	Z-average Particle Size (nm)	PDI	Drug recovery (%)	EE (%)	HSPC molar (M/M) %	CHOL molar (M/M) %	Drug molar (M/M) %
FEL1	175.7 ± 2.7	0.23 ± 0.03	108.3 ± 1.1	96.0 ± 1.6	62	18	20
FEL2	182.5 ± 2.8	0.25 ± 0.02	98.1 ± 2.8	94.5 ± 5.0	64.5	19	16.5
FEL3	184.7 ± 9.7	0.21 ± 0.03	95.0 ± 1.0	96.2 ± 3.1	63.2	18.8	18
FEL4	173.2 ± 7.3	0.23 ± 0.02	97.3 ± 0.8	98.3 ± 3.4	64	26	10

It has been widely reported that the cholesterol composition and chain length of the HSPC are significant for the rigidity of the liposomal nanocarriers (Monteiro et al., 2014). As the concentration of HSPC increases, the drug molecules' slower release is expected if they reside inside the bilayers rather than on the surface of the liposomes (Chobisa et al., 2018; Shaker et al., 2017). CHOL is vital in liposomal formulations; it dissolves into the lipid bilayer, impacting liposome stability, drug retention and particle size. The effects of CHOL on particle size and drug recovery of reconstituted liposomes are demonstrated in Table 2.

Further increases in CHOL had no significant impact on particle size, whilst the drug recovery and encapsulation efficiency increased when CHOL was increased from 15 – 25% w/w. A reduction in particle size upon the inclusion of CHOL has been reported previously and is due to interaction with the phospholipid bilayer, forming a more compact and rigid structure (Briuglia et al., 2015; Gangishetty et al., 2015). The results suggested a further increase in CHOL causes a tight packing of the phospholipid bilayers and more stable liposome nanoformulations. The final formulation parameter investigated was the concentration of drug molecules in relation to HSPC. It was seen that an increase in the drug concentration increased the particle size of the formulations. The particle size increase was significant in 10% to 40% w/w drug-loading liposomal formulations (Maritim et al., 2021). Hydrophobic drugs are loaded through dissolution into the phospholipid membrane, and as more drugs enter the bilayer, the particle size increases (Lee, 2020; Najlah et al., 2018). Above a 20% NPX loading, the size was not seen to increase significantly, which may be due to a maximum loading being reached with additional NPX dispersed into the hydrophilic carrier during the TSE process. The maximum drug loading capacity for NPX in HSPC-based liposomes at room temperature was predicted to be approximately 20%, supporting the findings. The particle size for FEL formulations showed a similar trend to that of NPX liposomal formulations. An increase in particle size was seen when the CHOL or HSPC concentration was increased. Unlike the NPX formulations, no significant changes were observed in particle size when the FEL loading was increased from 10 – 20% w/w with the HSPC liposomes, implying the maximum loading capacity of the drug using the TSE platform.

3.4 Drug release kinetics for NPX and FEL encapsulated liposomal nanoparticles

All the drug release studies were carried out over 24 hours under sink conditions. The drug release rates were compared within each formulation and across various drug loadings (Figure 10). As expected, pure NPX and FEL samples showed a full drug release (100%) over the test duration, confirming the sink condition of the settings. The physical mixtures of drugs with HSPC and cholesterol were also tested for NPX1 and FEL1 formulations, which showed immediate drug release profiles (Fan et al., 2021). A distinctive difference was observed for NPX and FEL HSPC-based liposomal nanoformulations: the NPX-HPSC system showed

immediate release kinetics, and the FEL-HPSC system showed slow and sustained release kinetics. Faster release kinetics and higher percentage release were obtained for NPX-containing liposomal nanoparticles than the FEL-HSPC systems, generating higher overall releases and maximum concentrations (Table 2). The maximum drug released in the NPX formulation was obtained at approximately 92% at 300 mins (NPX3), whilst the FEL formulation only released 26% of the initial drug content at 1440 mins (FEL1). Alternations of formulation compositions can lead to desired drug release kinetics within the respective drug-loaded liposomal nanoformulations. Based on a comparison of the release profiles of NPX3 and NPX4 over 1440 minutes, it appears that modifying the cholesterol and drug content (where NPX4 has half the amount of cholesterol and double the drug concentration compared to NPX3) does not have a significant impact on the extent of drug released by the end of the monitored period. Although NPX4 seems to reach its release plateau more quickly than NPX3, indicating a possibility of an increase in the initial release rate, the final percentage of drug released remains comparable between both formulations. This could suggest that the decrease in CHOL could improve the fluidity of the bilayer, which might help to accelerate the initial drug release rate (Shaker et al., 2017).

Interestingly, this drug-depended release profile is somehow indicated using the molecular dynamic and umbrella sampling simulations where a lower free energy barrier was estimated for the NPX-HSPC than FEL-HSPC. A lower free energy barrier between the drug and the HSPC bilayer can potentially lead to a high drug release rate, even though the global minimum is within the centre of the bilayer structure. At sink conditions, the driving force for NPX to diffuse out of the HSPC membrane is likely to exceed the free energy barrier in the NPX-HSPC system, hence higher drug release rate and lower drug retention (Svirkin et al., 2022). When comparing NPX1 and FEL1, which have similar molar ratios of HSPC and cholesterol to the drug, NPX exhibited a faster rate and greater extent of drug release than FEL. This difference may be due to the nature of the drug molecules' interaction with and localization within the liposomal bilayer structure. While NPX is likely to reside on the surface of the liposomes, FEL is thought to be localized closer to the lipid centre (as indicated by molecular modelling), suggesting that surface-associated drug molecules dissociate from the liposomal vesicles more rapidly, thereby providing faster release kinetics and a higher percentage of drug release.

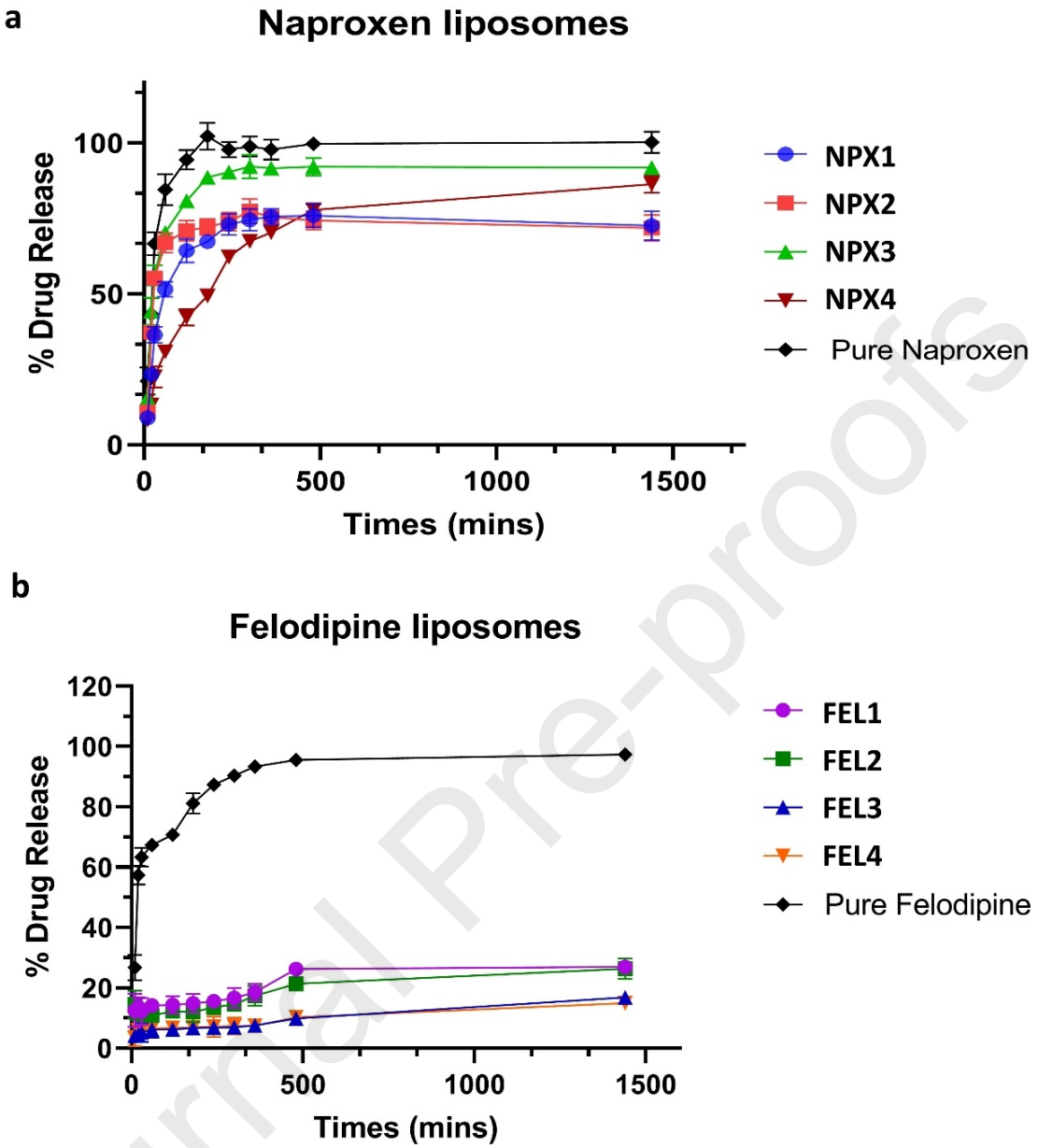

Figure 9 The drug release profiles of NPX (a) and FEL (b) HSPC liposomal nanoformulations for 24 hours under sink conditions. The actual % drug release as a function of time was calculated based on the average drug encapsulations after reconstitution (Table 2)

4. Conclusions

In this study, we have successfully integrated molecular dynamics simulations with thermodynamic modelling to investigate the interactions and phase behaviour of two drugs, naproxen and felodipine, with a phospholipid bilayer composed of hydrogenated soy phosphatidylcholine. This investigation provides a comprehensive understanding of drug

encapsulation and release mechanisms from liposomal nanocarriers, which are crucial for developing efficient drug delivery systems.

Specifically, we utilized umbrella sampling to calculate the free energy profiles for drug insertion and release from the HSPC bilayer. The results revealed distinct energy barriers associated with the permeation of naproxen and felodipine through the bilayer, indicating stark differences in their encapsulation efficiency and release kinetics. In particular, naproxen displayed a lower free energy barrier than felodipine, suggesting a more favourable interaction with the HSPC bilayer. The thermodynamic modelling, derived from melting point depression studies, confirmed the miscibility of the drugs with the lipid phase. Both drugs showed good miscibility with HSPC, with naproxen exhibiting stronger melting point depressions and stronger interactions with the lipid components. The Flory-Huggins thermodynamic modelling provided insight into the miscibility of drug-HSPC combinations over a range of temperatures and compositions. The phase diagrams constructed from these models guided the understanding of drug-phospholipid systems' behaviour, predicting the likelihood of drug encapsulation during the manufacturing process.

Moreover, stability studies, including PXRD, PLM, and DSC, validated the predictions from phase diagrams and confirmed the stability of the drug-phospholipid mixtures at the relevant drug loadings. Subsequently, we prepared liposomal formulations of naproxen and felodipine using a one-step twin-screw extrusion process, achieving encapsulation efficiencies and particle sizes that validate our computational predictions and thermodynamic modelling.

Finally, the release kinetics of naproxen and felodipine from the liposomal formulations were studied, demonstrating distinct release profiles. Naproxen showed immediate release kinetics, while felodipine exhibited slower, more sustained release, consistent with the molecular dynamics and umbrella sampling simulations' predictions.

In summary, this study's integration of computational and experimental approaches provides a robust framework for understanding and predicting the behaviour of drug-lipid systems in liposomal nanocarriers. The findings highlight the importance of molecular-level interactions and thermodynamic stability in the design of efficient drug delivery systems. Future research can extend these methodologies to other drugs and lipid compositions, enhancing liposomal nanocarriers' specificity and efficacy for drug delivery. This work contributes to the fundamental understanding of liposomal drug delivery mechanisms and offers a practical guide for designing optimized liposomal formulations for various therapeutic applications.

Acknowledgement

Funding: This work was supported, in part, by the Medical Research Council (*MR/X014010/1*).

Reference

Abascal, J.L.F., Sanz, E., Fernández, R.G., Vega, C., 2005a. A potential model for the study of ices and amorphous water: TIP4P/Ice. Journal of Chemical Physics 122. https://doi.org/10.1063/1.1931662

Abascal, J.L.F., Sanz, E., Fernández, R.G., Vega, C., 2005b. A potential model for the study of ices and amorphous water: TIP4P/Ice. Journal of Chemical Physics 122. https://doi.org/10.1063/1.1931662

Abraham, M.J., Murtola, T., Schulz, R., Páll, S., Smith, J.C., Hess, B., Lindah, E., 2015. Gromacs: High performance molecular simulations through multi-level parallelism from laptops to supercomputers. SoftwareX 1–2. https://doi.org/10.1016/j.softx.2015.06.001

Akbarzadeh, A., Rezaei-sadabady, R., Davaran, S., Joo, S.W., Zarghami, N., 2013. Liposome : classification , preparation , and applications. Nanoscale Res Lett 8, 1. https://doi.org/10.1186/1556-276X-8-102

Akinc, A., Maier, M.A., Manoharan, M., Fitzgerald, K., Jayaraman, M., Barros, S., Ansell, S., Du, X., Hope, M.J., Madden, T.D., Mui, B.L., Semple, S.C., Tam, Y.K., Ciufolini, M., Witzigmann, D., Kulkarni, J.A., van der Meel, R., Cullis, P.R., 2019. The Onpattro story and the clinical translation of nanomedicines containing nucleic acid-based drugs. Nat Nanotechnol. https://doi.org/10.1038/s41565-019-0591-y

Andrews, G.P., Abu-Diak, O., Kusmanto, F., Hornsby, P., Hui, Z., Jones, D.S., 2010. Physicochemical characterization and drug-release properties of celecoxib hot-melt extruded glass solutions. Journal of Pharmacy and Pharmacology 62, 1580–1590. https://doi.org/10.1111/j.2042-7158.2010.01177.x

Andrews, G.P., Qian, K., Jacobs, E., Jones, D.S., Tian, Y., 2023. High drug loading nanosized amorphous solid dispersion (NASD) with enhanced in vitro solubility and permeability: Benchmarking conventional ASD. Int J Pharm 632, 122551. https://doi.org/10.1016/j.ijpharm.2022.122551

Baird, J.A., Taylor, L.S., 2012. Evaluation of amorphous solid dispersion properties using thermal analysis techniques. Adv Drug Deliv Rev 64, 396–421. https://doi.org/10.1016/j.addr.2011.07.009

Bakshi, R.P., Tatham, L.M., Savage, A.C., Tripathi, A.K., Mlambo, G., Ippolito, M.M., Nenortas, E., Rannard, S.P., Owen, A., Shapiro, T.A., 2018. Long-acting injectable atovaquone nanomedicines for malaria prophylaxis. Nat Commun 315. https://doi.org/10.1038/s41467-017-02603-z

Bandara, S.R., Molley, T.G., Kim, H., Bharath, P.A., Kilian, K.A., Leal, C., 2020. The structural fate of lipid nanoparticles in the extracellular matrix. Mater Horiz 7, 125–134. https://doi.org/10.1039/c9mh00835g

Barenholz, Y., 2012. Doxil - The first FDA-approved nano-drug: Lessons learned. Journal of Controlled Release 160, 117–134. https://doi.org/10.1016/j.jconrel.2012.03.020

Beltrán-Gracia, E., López-Camacho, A., Higuera-Ciapara, I., Velázquez-Fernández, J.B., Vallejo-Cardona, A.A., 2019. Nanomedicine review: Clinical developments in liposomal applications. Cancer Nanotechnol. https://doi.org/10.1186/s12645-019-0055-y

Berendsen, H.J.C., Postma, J.P.M., Van Gunsteren, W.F., Dinola, A., Haak, J.R., 1984. Molecular dynamics with coupling to an external bath. J Chem Phys 81. https://doi.org/10.1063/1.448118

Bern, C., Adler-Moore, J., Berenguer, J., Boelaert, M., Boer, M. den, Davidson, R.N., Figueras, C., Gradoni, L., Kafetzis, D.A., Ritmeijer, K., Rosenthal, E., Royce, C., Russo, R., Sundar, S., Alvar, J., 2006. Liposomal Amphotericin B for the Treatment of Visceral Leishmaniasis. Clinical Infectious Diseases 43, 917–924. https://doi.org/10.1086/507530

Bhakat, S., 2022. Collective variable discovery in the age of machine learning: reality, hype and everything in between. RSC Adv. https://doi.org/10.1039/d2ra03660f

Boddu, M., Choppari, V., Rapalli, V.K., Badam, M., 2017. Formulation and Evaluation of Proniosomes of Felodipine. Drug Des 06, 1–9. https://doi.org/10.4172/2169-0138.1000154

Bonnans, C., Chou, J., Werb, Z., 2014. Remodelling the extracellular matrix in development and disease. Nat Rev Mol Cell Biol. https://doi.org/10.1038/nrm3904

Briuglia, M.L., Rotella, C., McFarlane, A., Lamprou, D.A., 2015. Influence of cholesterol on liposome stability and on in vitro drug release. Drug Deliv Transl Res 5, 231–242. https://doi.org/10.1007/s13346-015-0220-8

Brooks, B.R., Brooks, C.L., Mackerell, A.D., Nilsson, L., Petrella, R.J., Roux, B., Won, Y., Archontis, G., Bartels, C., Boresch, S., Caflisch, A., Caves, L., Cui, Q., Dinner, A.R., Feig, M., Fischer, S., Gao, J., Hodoscek, M., Im, W., Kuczera, K., Lazaridis, T., Ma, J., Ovchinnikov, V., Paci, E., Pastor, R.W., Post, C.B., Pu, J.Z., Schaefer, M., Tidor, B., Venable, R.M., Woodcock, H.L., Wu, X., Yang, W., York, D.M., Karplus, M., 2009. CHARMM: The biomolecular simulation program. J Comput Chem 30. https://doi.org/10.1002/jcc.21287

Bunker, A., Magarkar, A., Viitala, T., 2016. Rational design of liposomal drug delivery systems, a review: Combined experimental and computational studies of lipid membranes, liposomes and their PEGylation. Biochim Biophys Acta Biomembr 1858. https://doi.org/10.1016/j.bbamem.2016.02.025

Bussi, G., Donadio, D., Parrinello, M., 2007. Canonical sampling through velocity rescaling. Journal of Chemical Physics 126. https://doi.org/10.1063/1.2408420

Cárdenas, M., Campbell, R.A., Yanez Arteta, M., Lawrence, M.J., Sebastiani, F., 2023. Review of structural design guiding the development of lipid nanoparticles for nucleic acid delivery. Curr Opin Colloid Interface Sci. https://doi.org/10.1016/j.cocis.2023.101705

Chang, H. -C, Flanagan, D.R., 1995. Liposomal entrapment of suramin(II): Interaction of suramin with phospholipids of various chain lengths. J Pharm Sci 84, 1078–1082. https://doi.org/10.1002/jps.2600840909

Chobisa, D., Patel, K., Monpara, J., Patel, M., Vavia, P., 2018. Development and characterization of an organic solvent free, proliposomal formulation of Busulfan using quality by design approach. Int J Pharm 535, 360–370. https://doi.org/10.1016/j.ijpharm.2017.11.007

Clifton, L.A., Campbell, R.A., Sebastiani, F., Campos-Terán, J., Gonzalez-Martinez, J.F., Björklund, S., Sotres, J., Cárdenas, M., 2020. Design and use of model membranes to study biomolecular interactions using complementary surface-sensitive techniques. Adv Colloid Interface Sci. https://doi.org/10.1016/j.cis.2020.102118

Dan, N., 2015. Drug release through liposome pores. Colloids Surf B Biointerfaces 126. https://doi.org/10.1016/j.colsurfb.2014.11.042

Dave, H., Gao, F., Lee, J.H., Liberatore, M., Ho, C.C., Co, C.C., 2007. Self-assembly in sugar-oil complex glasses. Nat Mater 6, 287–290. https://doi.org/10.1038/nmat1864

Donnelly, C., Tian, Y., Potter, C.C.C., Jones, D.S.D.S., Andrews, G.P.G.P., 2014. Probing the Effects of Experimental Conditions on the Character of Drug-Polymer Phase Diagrams Constructed Using Flory-Huggins Theory. Pharm Res 32, 167–179. https://doi.org/10.1007/s11095-014-1453-9

Duangjit, S., Pamornpathomkul, B., Opanasopit, P., Rojanarata, T., Obata, Y., Takayama, K., Ngawhirunpat, T., 2014. Role of the charge, carbon chain length, and content of surfactant on the skin penetration of meloxicam-loaded liposomes. Int J Nanomedicine 9, 2005–2017. https://doi.org/10.2147/IJN.S60674

El Maghraby, G.M.M., Williams, A.C., Barry, B.W., 2005. Drug interaction and location in liposomes: Correlation with polar surface areas. Int J Pharm 292, 179–185. https://doi.org/10.1016/j.ijpharm.2004.11.037

Eze, M.O., 1991. Phase transitions in phospholipid bilayers: Lateral phase separations play vital roles in biomembranes. Biochem Educ 19, 204–208. https://doi.org/10.1016/0307-4412(91)90103-F

Fan, L., Chen, Q., Mairiyangu, Y., Wang, Y., Liu, X., 2021. Stable vesicle self-assembled from phospholipid and mannosylerythritol lipid and its application in encapsulating anthocyanins. Food Chem 344, 128649. https://doi.org/10.1016/j.foodchem.2020.128649

Farokhzad, O.C., Langer, R., 2009. Impact of Nanotechnology on Drug. American Chemical Society Nano 3, 16–20.
Fearon, A.D., Stokes, G.Y., 2017. Thermodynamics of Indomethacin Adsorption to Phospholipid Membranes. Journal of Physical Chemistry B 121. https://doi.org/10.1021/acs.jpcb.7b08359
Gangishetty, H., Eedara, B.B., Bandari, S., 2015. Development of ketoprofen loaded proliposomal powders for improved gastric absorption and gastric tolerance: In vitro and in situ evaluation. Pharm Dev Technol 20, 641–651. https://doi.org/10.3109/10837450.2014.908306
Giardiello, M., Liptrott, N.J., McDonald, T.O., Moss, D., Siccardi, M., Martin, P., Smith, D., Gurjar, R., Rannard, S.P., Owen, A., 2016. Accelerated oral nanomedicine discovery from miniaturized screening to clinical production exemplified by paediatric HIV nanotherapies. Nat Commun 7, 1–10. https://doi.org/10.1038/ncomms13184
Go, M.L., Ngiam, T.L., 1997. Thermodynamics of partitioning of the antimalarial drug mefloquine in phospholipid bilayers and bulk solvents. Chem Pharm Bull (Tokyo) 45. https://doi.org/10.1248/cpb.45.2055
Grossfield, A., 2022. WHAM: the weighted histogram analysis method", version 2.0.11 [WWW Document]. http://membrane.urmc.rochester.edu/?page_id=126.
Hengsawas Surasarang, S., Keen, J.M., Huang, S., Zhang, F., McGinity, J.W., Williams, R.O., 2017. Hot melt extrusion versus spray drying: hot melt extrusion degrades albendazole. Drug Dev Ind Pharm 43, 797–811. https://doi.org/10.1080/03639045.2016.1220577
Hess, B., Bekker, H., Berendsen, H.J.C., Fraaije, J.G.E.M., 1997. LINCS: A Linear Constraint Solver for molecular simulations. J Comput Chem 18. https://doi.org/10.1002/(SICI)1096-987X(199709)18:12<1463::AID-JCC4>3.0.CO;2-H
Hou, X., Zaks, T., Langer, R., Dong, Y., 2021. Lipid nanoparticles for mRNA delivery. Nat Rev Mater. https://doi.org/10.1038/s41578-021-00358-0
Hub, J.S., De Groot, B.L., Van Der Spoel, D., 2010. G-whams-a free Weighted Histogram Analysis implementation including robust error and autocorrelation estimates. J Chem Theory Comput 6. https://doi.org/10.1021/ct100494z
Ianiro, A., Wu, H., van Rijt, M.M.J., Vena, M.P., Keizer, A.D.A., Esteves, A.C.C., Tuinier, R., Friedrich, H., Sommerdijk, N.A.J.M., Patterson, J.P., 2019. Liquid–liquid phase separation during amphiphilic self-assembly. Nat Chem 11, 320–328. https://doi.org/10.1038/s41557-019-0210-4
Jabbari, V., Sawczyk, M., Amiri, A., Král, P., Shahbazian-Yassar, R., 2023. Unveiling growth and dynamics of liposomes by graphene liquid cell-transmission electron microscopy. Nanoscale 15. https://doi.org/10.1039/d2nr06147c
Jacobs, E., Qian, K., Pietsch, V.L., Richter, M., Jones, D.S., Andrews, G.P., Tian, Y., 2022. Design and scale-up of amorphous drug nanoparticles production via a one-step anhydrous continuous process. Int J Pharm 628. https://doi.org/10.1016/j.ijpharm.2022.122304
Jämbeck, J.P.M., Eriksson, E.S.E., Laaksonen, A., Lyubartsev, A.P., Eriksson, L.A., 2014. Molecular dynamics studies of Liposomes as carriers for photosensitizing drugs: Development, validation, and simulations with a coarse-grained model. J Chem Theory Comput 10, 5–13. https://doi.org/10.1021/ct400466m
Janssen products, L.P., 2013. All about Doxil [WWW Document]. http://www.doxil.com/.
Jo, S., Kim, T., Iyer, V.G., Im, W., 2008. CHARMM-GUI: A web-based graphical user interface for CHARMM. J Comput Chem 29. https://doi.org/10.1002/jcc.20945
Jo, S., Lim, J.B., Klauda, J.B., Im, W., 2009. CHARMM-GUI membrane builder for mixed bilayers and its application to yeast membranes. Biophys J 97. https://doi.org/10.1016/j.bpj.2009.04.013
Kabanov, A V; Gendelman, H.E., 2007. Nanomedicine in the diagnosis and therapy of neurodegenerative disorders. Prog Polym Sci 32, 1054–1082. https://doi.org/10.1016/j.progpolymsci.2007.05.014.Nanomedicine

Kassem, M.A., Aboul-Einien, M.H., El Taweel, M.M., 2018. Dry Gel Containing Optimized Felodipine-Loaded Transferosomes: a Promising Transdermal Delivery System to Enhance Drug Bioavailability. AAPS PharmSciTech 19, 2155–2173. https://doi.org/10.1208/s12249-018-1020-5

Kisby, T., Yilmazer, A., Kostarelos, K., 2021. Reasons for success and lessons learnt from nanoscale vaccines against COVID-19. Nat Nanotechnol. https://doi.org/10.1038/s41565-021-00946-9

Kluzek, M., Oppenheimer-Shaanan, Y., Dadosh, T., Morandi, M.I., Avinoam, O., Raanan, C., Goldsmith, M., Goldberg, R., Klein, J., 2022. Designer Liposomic Nanocarriers Are Effective Biofilm Eradicators. ACS Nano 16, 15792–15804. https://doi.org/10.1021/acsnano.2c04232

Koch, C.C., Jang, J.S.C., Gross, S.S., 1989. The melting point depression of tin in mechanically milled tin and germanium powder mixtures. J Mater Res 4, 557–564. https://doi.org/10.1557/JMR.1989.0557

Lee, J., Cheng, X., Swails, J.M., Yeom, M.S., Eastman, P.K., Lemkul, J.A., Wei, S., Buckner, J., Jeong, J.C., Qi, Y., Jo, S., Pande, V.S., Case, D.A., Brooks, C.L., MacKerell, A.D., Klauda, J.B., Im, W., 2016. CHARMM-GUI Input Generator for NAMD, GROMACS, AMBER, OpenMM, and CHARMM/OpenMM Simulations Using the CHARMM36 Additive Force Field. J Chem Theory Comput 12. https://doi.org/10.1021/acs.jctc.5b00935

Lee, M.K., 2020. Liposomes for enhanced bioavailability of water-insoluble drugs: In vivo evidence and recent approaches. Pharmaceutics 12, 264. https://doi.org/10.3390/pharmaceutics12030264

Li, X., Cooper, M.A., 2012. Measurement of drug lipophilicity and pK a using acoustics. Anal Chem 84, 2609–2613. https://doi.org/10.1021/ac300087z

Li, Z., Kang, H., Che, N., Liu, Z., Li, P., Li, W., Zhang, C., Cao, C., Liu, R., Huang, Y., 2014. Controlled release of liposome-encapsulated Naproxen from core-sheath electrospun nanofibers. Carbohydr Polym 111, 18–24. https://doi.org/10.1016/j.carbpol.2014.04.017

MacKerell, A.D., Bashford, D., Bellott, M., Dunbrack, R.L., Evanseck, J.D., Field, M.J., Fischer, S., Gao, J., Guo, H., Ha, S., Joseph-McCarthy, D., Kuchnir, L., Kuczera, K., Lau, F.T.K., Mattos, C., Michnick, S., Ngo, T., Nguyen, D.T., Prodhom, B., Reiher, W.E., Roux, B., Schlenkrich, M., Smith, J.C., Stote, R., Straub, J., Watanabe, M., Wiórkiewicz-Kuczera, J., Yin, D., Karplus, M., 1998. All-atom empirical potential for molecular modeling and dynamics studies of proteins. Journal of Physical Chemistry B 102. https://doi.org/10.1021/jp973084f

Mantsch, H.H., McElhaney, R.N., 1991. Phospholipid phase transitions in model and biological membranes as studied by infrared spectroscopy. Chem Phys Lipids 57. https://doi.org/10.1016/0009-3084(91)90077-O

Marcos, X., Sixto-López, Y., Pérez-Casas, S., Correa-Basurto, J., 2022. Computational study of DMPC liposomes loaded with the N-(2-Hydroxyphenyl)-2-propylpentanamide (HO-AAVPA) and determination of its antiproliferative activity in vitro in NIH-3T3 cells. J Biomol Struct Dyn. https://doi.org/10.1080/07391102.2021.1955744

Maritim, S., Boulas, P., Lin, Y., 2021. Comprehensive analysis of liposome formulation parameters and their influence on encapsulation, stability and drug release in glibenclamide liposomes. Int J Pharm 592, 120051. https://doi.org/10.1016/j.ijpharm.2020.120051

Mehnert, W., Maeder, K., 2012. Solid lipid nanoparticles Production, characterization and applications. Adv Drug Deliv Rev 64, 83–101. https://doi.org/10.1016/j.addr.2012.09.021

Meng, F., Trivino, A., Prasad, D., Chauhan, H., 2015. Investigation and correlation of drug polymer miscibility and molecular interactions by various approaches for the preparation of amorphous solid dispersions. European Journal of Pharmaceutical Sciences 71, 12–24. https://doi.org/10.1016/j.ejps.2015.02.003

Meyerhoff, A., 1999. U.S. Food and Drug Administration Approval of AmBisome (Liposomal Amphotericin B) for Treatment of Visceral Leishmaniasis. Clinical Infectious Diseases 28, 49–51. https://doi.org/10.1086/515086

Midya, U.S., Bandyopadhyay, S., 2014. Hydration behavior at the ice-binding surface of the tenebrio molitor antifreeze protein. Journal of Physical Chemistry B 118. https://doi.org/10.1021/jp412528b

Miles, C.M., Hsu, P.C., Dixon, A.M., Khalid, S., Sosso, G.C., 2022. Lipid bilayers as potential ice nucleating agents. Physical Chemistry Chemical Physics 24. https://doi.org/10.1039/d1cp05465a

Miyamoto, S., Kollman, P.A., 1992. Settle: An analytical version of the SHAKE and RATTLE algorithm for rigid water models. J Comput Chem 13. https://doi.org/10.1002/jcc.540130805

Mohammed, A.R., Weston, N., Coombes, A.G.A., Fitzgerald, M., Perrie, Y., 2004. Liposome formulation of poorly water soluble drugs: Optimization of drug loading and ESEM analysis of stability. Int J Pharm 285, 23–34. https://doi.org/10.1016/j.ijpharm.2004.07.010

Monteiro, N., Martins, A., Reis, R.L., Neves, N.M., 2014. Liposomes in tissue engineering and regenerative medicine. J R Soc Interface. https://doi.org/10.1098/rsif.2014.0459

Najlah, M., Jain, M., Wan, K.W., Ahmed, W., Albed Alhnan, M., Phoenix, D.A., Taylor, K.M.G., Elhissi, A., 2018. Ethanol-based proliposome delivery systems of paclitaxel for in vitro application against brain cancer cells. J Liposome Res 28, 74–85. https://doi.org/10.1080/08982104.2016.1259628

Niskanen, J., Tenhu, H., 2017. How to manipulate the upper critical solution temperature (UCST)? Polym Chem 8, 220–232. https://doi.org/10.1039/c6py01612j

Nutt, D.R., Smith, J.C., 2007. Molecular dynamics simulations of proteins: Can the explicit water model be varied? J Chem Theory Comput 3. https://doi.org/10.1021/ct700053u

Paracini, N., Gutfreund, P., Welbourn, R., Gonzalez-Martinez, J.F., Zhu, K., Miao, Y., Yepuri, N., Darwish, T.A., Garvey, C., Waldie, S., Larsson, J., Wolff, M., Cárdenas, M., 2023. Structural Characterization of Nanoparticle-Supported Lipid Bilayer Arrays by Grazing Incidence X-ray and Neutron Scattering. ACS Appl Mater Interfaces 15. https://doi.org/10.1021/acsami.2c18956

Parchekani, J., Allahverdi, A., Taghdir, M., Naderi-Manesh, H., 2022. Design and simulation of the liposomal model by using a coarse-grained molecular dynamics approach towards drug delivery goals. Sci Rep 12. https://doi.org/10.1038/s41598-022-06380-8

Park, K., 2016. Drug delivery of the future: Chasing the invisible gorilla. Journal of Controlled Release 240. https://doi.org/10.1016/j.jconrel.2015.10.048

Park, K., 2013. Facing the truth about nanotechnology in drug delivery. ACS Nano. https://doi.org/10.1021/nn404501g

Peer, D., Karp, J.M., Hong, S., Farokhzad, O.C., Margalit, R., Langer, R., 2007. Nanocarriers as an emerging platform for cancer therapy. Nat Nanotechnol. https://doi.org/10.1038/nnano.2007.387

Pereira, S., Ma, G., Na, L., Hudoklin, S., Kreft, M.E., Kostevsek, N., Al-Jamal, W.T., 2022. Encapsulation of doxorubicin prodrug in heat-triggered liposomes overcomes off-target activation for advanced prostate cancer therapy. Acta Biomater 140, 530–546. https://doi.org/10.1016/j.actbio.2021.12.019

Pronk, S., Páll, S., Schulz, R., Larsson, P., Bjelkmar, P., Apostolov, R., Shirts, M.R., Smith, J.C., Kasson, P.M., Van Der Spoel, D., Hess, B., Lindahl, E., 2013. GROMACS 4.5: A high-throughput and highly parallel open source molecular simulation toolkit. Bioinformatics 29. https://doi.org/10.1093/bioinformatics/btt055

Rivnay, B., Wakim, J., Avery, K., Petrochenko, P., Myung, J.H., Kozak, D., Yoon, S., Landrau, N., Nivorozhkin, A., Hye, J., Kozak, D., Yoon, S., Landrau, N., Nivorozhkin, A., 2019. Critical process parameters in manufacturing of liposomal formulations of amphotericin B. Int J Pharm 565, 447–457. https://doi.org/10.1016/j.ijpharm.2019.04.052

Schiener, M., Hossann, M., Viola, J.R., Ortega-Gomez, A., Weber, C., Lauber, K., Lindner, L.H., Soehnlein, O., 2014. Nanomedicine-based strategies for treatment of atherosclerosis. Trends Mol Med 20, 271–281. https://doi.org/10.1016/j.molmed.2013.12.001

Shah, S., Dhawan, V., Holm, R., Nagarsenker, M.S., Perrie, Y., 2020. Liposomes: Advancements and innovation in the manufacturing process. Adv Drug Deliv Rev 154–155, 102–122. https://doi.org/10.1016/j.addr.2020.07.002

Shaker, S., Gardouh, A., Ghorab, M., 2017. Factors affecting liposomes particle size prepared by ethanol injection method. Res Pharm Sci 12, 346–352. https://doi.org/10.4103/1735-5362.213979

Shi, J., Kantoff, P.W., Wooster, R., Farokhzad, O.C., 2017. Cancer nanomedicine: Progress, challenges and opportunities. Nat Rev Cancer. https://doi.org/10.1038/nrc.2016.108

Siani, P., Donadoni, E., Ferraro, L., Re, F., Di Valentin, C., 2022. Molecular dynamics simulations of doxorubicin in sphingomyelin-based lipid membranes. Biochim Biophys Acta Biomembr 1864. https://doi.org/10.1016/j.bbamem.2021.183763

Soteras Gutiérrez, I., Lin, F.Y., Vanommeslaeghe, K., Lemkul, J.A., Armacost, K.A., Brooks, C.L., MacKerell, A.D., 2016. Parametrization of halogen bonds in the CHARMM general force field: Improved treatment of ligand–protein interactions. Bioorg Med Chem 24. https://doi.org/10.1016/j.bmc.2016.06.034

Stone, N.R.H., Bicanic, T., Salim, R., Hope, W., 2016. Liposomal Amphotericin B (AmBisome®): A Review of the Pharmacokinetics, Pharmacodynamics, Clinical Experience and Future Directions. Drugs. https://doi.org/10.1007/s40265-016-0538-7

Sultana, S.S., Sailaja, A.K., 2017. Preparation and evaluation of naproxen sodium loaded liposomes, ethosomes and transferosomes. Journal of Bionanoscience 11, 284–291. https://doi.org/10.1166/jbns.2017.1448

Svirkin, Y., Lee, J., Marx, R., Yoon, S., Landrau, N., Kaisar, M.A., Qin, B., Park, J.H., Alam, K., Kozak, D., Wang, Y., Xu, X., Zheng, J., Rivnay, B., 2022. Amphotericin B release rate is the link between drug status in the liposomal bilayer and toxicity. Asian J Pharm Sci 0–44. https://doi.org/10.1016/j.ajps.2022.04.007

Tang, J., Srinivasan, S., Yuan, W., Ming, R., Liu, Y., Dai, Z., Noble, C.O., Hayes, M.E., Zheng, N., Jiang, W., Szoka, F.C., Schwendeman, A., 2019. Development of a flow-through USP 4 apparatus drug release assay for the evaluation of amphotericin B liposome. European Journal of Pharmaceutics and Biopharmaceutics 134, 107–116. https://doi.org/10.1016/j.ejpb.2018.11.010

Tian, Y., Booth, J., Meehan, E., Jones, D.S.D.S., Li, S., Andrews, G.P.G.P., 2013. Construction of drug-polymer thermodynamic phase diagrams using flory-huggins interaction theory: Identifying the relevance of temperature and drug weight fraction to phase separation within solid dispersions. Mol Pharm 10, 236–248. https://doi.org/10.1021/mp300386v

Tian, Y., Jacobs, E., Jones, D.S., McCoy, C.P., Wu, H., Andrews, G.P., 2020. The design and development of high drug loading amorphous solid dispersion for hot-melt extrusion platform. Int J Pharm 586, 1–43. https://doi.org/10.1016/j.ijpharm.2020.119545

Torrie, G.M., Valleau, J.P., 1977. Nonphysical sampling distributions in Monte Carlo free-energy estimation: Umbrella sampling. J Comput Phys 23. https://doi.org/10.1016/0021-9991(77)90121-8

Torrie, G.M., Valleau, J.P., 1974. Monte Carlo free energy estimates using non-Boltzmann sampling: Application to the sub-critical Lennard-Jones fluid. Chem Phys Lett 28. https://doi.org/10.1016/0009-2614(74)80109-0

Tromans, R.A., Carter, T.S., Chabanne, L., Crump, M.P., Li, H., Matlock, J. V., Orchard, M.G., Davis, A.P., 2018. A biomimetic receptor for glucose. Nat Chem 11. https://doi.org/10.1038/s41557-018-0155-z

Vanommeslaeghe, K., Hatcher, E., Acharya, C., Kundu, S., Zhong, S., Shim, J., Darian, E., Guvench, O., Lopes, P., Vorobyov, I., Mackerell, A.D., 2010. CHARMM general force

field: A force field for drug-like molecules compatible with the CHARMM all-atom additive biological force fields. J Comput Chem 31. https://doi.org/10.1002/jcc.21367
Veiseh, O., Tang, B.C., Whitehead, K.A., Daniel, G., Langer, R., 2016. Managing diabetes with nanomedicine: challenges and opportunities. Nat. Rev. Drug Discov. 14, 45–57. https://doi.org/10.1038/nrd4477.Managing
Xing, H., Hwang, K., Lu, Y., 2016. Recent developments of liposomes as nanocarriers for theranostic applications. Theranostics. https://doi.org/10.7150/thno.15464
Yao, X., Fan, X., Yan, N., 2020. Cryo-EM analysis of a membrane protein embedded in the liposome. Proc Natl Acad Sci U S A 117. https://doi.org/10.1073/pnas.2009385117
Yeh, I.C., Berkowitz, M.L., 1999. Ewald summation for systems with slab geometry. Journal of Chemical Physics 111. https://doi.org/10.1063/1.479595

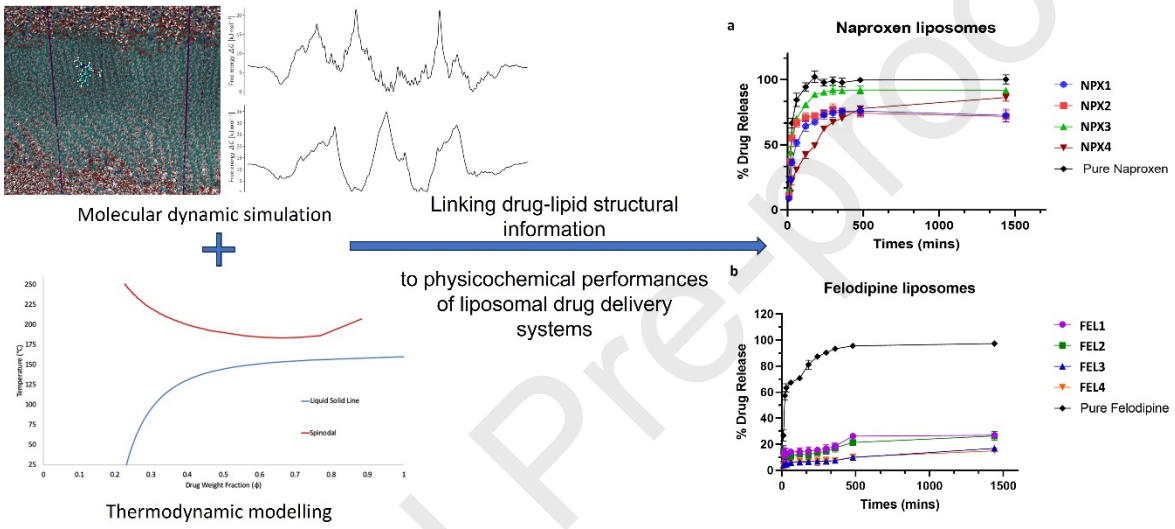

Declaration of interests

☒ The authors declare that they have no known competing financial interests or personal relationships that could have appeared to influence the work reported in this paper.

☐ The authors declare the following financial interests/personal relationships which may be considered as potential competing interests: